Journal of Thermal Stresses, 28: 1031–1065, 2005

ISSN: 0149-5739 print/1521-074X online
DOI: 10.1080/01495730590964963

Taylor & Francis
Taylor & Francis Group

UNIFIED FORMULATION FOR FINITE ELEMENT THERMOELASTIC ANALYSIS OF MULTILAYERED ANISOTROPIC COMPOSITE PLATES

A. Robaldo and E. Carrera
DIASP Politecnico di Torino, Turin, Italy

A. Benjeddou
Institut Supérieur de Mécanique de Paris, Paris, France

This article presents various finite plate elements for the thermal stress analysis of multilayered anisotropic structures. Assumptions are made for the displacement fields in thickness direction and the principle of virtual displacements (PVD) is employed to derive finite element (FE) matrices. The unified formulation is employed so that these FE matrices have been derived in terms of a few fundamental nuclei whose form is not affected by number of the nodes of the elements or order of the expansion for the displacements-variable description (layer-wise (LW) and equivalent single layer (ESL) cases are both addressed). The Murakami zig-zag function is used to introduce zig-zag effects in the framework of ESL descriptions. The performances of the derived finite elements, in terms of displacement and stress fields, are shown by solving thermal stress problems related to cross-ply laminated plates for various thickness ratio values. Comparison to closed form solutions as well as to available 3-D exact analyses have shown the effectiveness of the proposed elements and their capability to trace quasi 3-D descriptions of thermal stresses in layered plates.

INTRODUCTION

Temperature variations often represent a contributing factor and sometimes even the predominant cause of failure of engineering structures. These structures often consist of beams, plates, shells, etc., that are made of multilayered materials. Some examples of multilayered materials can be found in the advanced composite materials that were developed for aerospace vehicles (launching/reentry vehicles and fighter aircraft) during the second part of the last century. Biomedical retina, reactor vessels, turbines, advanced optical mirrors, semiconductor technologies, and space antennas are further examples of multilayered structures that can be subjected to severe thermal environments.

An adequate knowledge of the deflections and stresses induced by thermal loads in these structures is of prime interest for structural analysts. The excessive

Communicated by Liviu Librescu on November 25, 2004.
Address correspondence to Erasmo Carrera, Aerospace Department, Politecnico di Torino, Corso Duca degli Abruzzi 24, 10129, Torino, Italy. E-mail: erasmo.carrera@polito.it

stress levels caused by temperature are, in fact, often the predominant cause of failure of laminated composite structures. Some significant problems of thermal stresses have been treated by Librescu et al. [1–8]. Elevated thermal stresses at layer interfaces constitute the origin of failure mechanisms such as the debonding of layers and the development of longitudinal cracks. Thus, an accurate description of local stress fields in each layer becomes mandatory in the first stages of the design.

The thermal bending of homogeneous anisotropic thin plates was first studied by Pell [9]. Later, Stavsky [10] developed a thermoelastic theory for heterogeneous anisotropic plates subjected to arbitrary three-dimensional (3-D) temperature distribution. Thermal deformations and related stresses for symmetric and antisymmetric rectangular laminates have been investigated by Wu and Tauchert [11–12] using classical laminated theory (CLT). Such models based on the Kirchhoff assumptions are adequate to predict the gross behavior of thin plates, but for moderately thick and thick plates, the transverse shear deformation effect has to be incorporated. Reddy and Hsu [13] presented both a closed form solution and a finite element model extending the first-order shear deformation theory (FSDT) developed by Whitney and Pagano [14] to laminated plates subjected to thermal and mechanical loadings. However, these classical models are not able to reproduce what is known as the zig-zag (ZZ) effect for the displacement fields and interlaminar continuity (IC), for transverse stresses. Carrera [15–16] summarized and IC by introducing the acronyms C_z^0 requirements. That is, both displacement and transverse stresses must be C^0 continuous functions in the thickness z direction; displacement and transverse stresses present discontinuous first derivatives with correspondence to each interface where the mechanical properties change. The fulfillment of C_z^0 requirements is a crucial point of two-dimensional modeling of multilayered structures. Many amendments to classical theories have been proposed to partially fulfill the C_z^0 requirements; see Carrera [16–17]. A few contributions to thermal stress problems are discussed below.

He [18] presented a layer-wise (LW) shear deformation theory for the analysis of steady-state thermal stresses showing that discrete-layer models in which the number of variables depends on the number of layers provides better predictions than the previously equivalent single layer (ESL) models in which a single displacement field is assumed throughout the whole laminate thickness. The superiority of the layer-wise description of the unknowns had been already emphasized by Murakami [19]. Higher-order theories for the thermal analysis of laminated plates have been reported by Cho et al. [20] and Kheider and Reddy [21], among others.

Several analytical solutions of the three-dimensional equations of thermoelasticity have been presented by Srinivas and Rao [22], Bapu Rao [23], Murakami [19], Bhaskar and Varadan [24], and Ali et al. [25]. Tungikar and Rao [26], Noor et al. [27], and Savoia and Reddy [28] developed an exact solution for thermal stresses in simply supported anisotropic laminates. Recently, Vel and Batra [29] have used a series solution for addressing the generalized plane strain and the three-dimensional deformations of laminated elastic plates subjected to thermal loads and arbitrary boundary conditions.

A possible way to a priori fulfill the C_z^0 requirements without any post-processing procedure (such as those used in most of the available analyses) is to refer to mixed formulation [30]. In that article Carrera introduced a unified formulation for the thermomechanical analysis of multilayered plates. In particular, the governing

equations of thermoelasticity were derived for the classical principle of virtual displacement (PVD) and the Reissner's mixed variational principle (RMVT); the description of the unknowns were applied at each layer separately (LW) and to the whole laminate (ESL). In addition the order of the expansion of the unknowns was taken as a free parameter. To overcome the limitations typical of analytical solutions such as those on the geometry and the boundary conditions, finite elements based on this formulation have been already introduced by Carrera and Demasi [31] for mechanical loads with satisfactory results. A detailed description of the unified formulation was provided by Carrera [32]. The present work aims to show the potential of the aforementioned unified formulation of multilayered plates to develop finite plate elements for thermoelastic analysis. The work Carrera and Demasi [31] is therefore extended to thermal problems. Attention has been restricted to displacement formulation and PVD applications. Extension to a mixed formulation based on RMVT will be proposed in a future article. The accuracy of the present model is verified comparing the obtained results to available 3-D exact solutions as well as to related closed form solutions in the literature.

GEOMETRY OF MULTILAYERED PLATES AND MATERIAL ASSUMPTIONS

A multilayered plate is a laminate obtained by stacking rectangular layers until the desired thickness and stiffness are reached. Generally each layer can be made of any kind of material, but in this work fiber-reinforced composites are considered. In particular, our interest will be focused on laminates made by unidirectional fiber-reinforced laminae, thus, as usual, they are considered homogeneous and operating in the linear elastic range, while the material is taken as orthotropic. The term unidirectional indicates that in each lamina all the fibers are aligned in the same direction. In general, each lamina can feature a different ply angle and this permits designing the right stiffness and strength to match the structural requirements. The sequence of the various laminae orientations is referred to as the *stacking sequence*. An in-depth description of laminated structures can be found in Reddy.

To analyze such a typology of structures, two different coordinate systems should be introduced: the material and the laminate. The first one is given for each lamina and is commonly indicated by the axes 1, 2, 3. The material coordinate 1-axis is taken to be parallel to the fiber direction, the 2-axis is transverse to the fiber direction in the plane of the lamina, and the 3-axis is perpendicular to the lamina. The laminate coordinate system, indicated by the axes x, y, z is shown in Figure 1 for a plate with three layers and dimensions a, b, and h. All the material data, such as Young's moduli and temperature-stress coefficients, are given in the material reference system, and the analysis of the structure is made in the laminate coordinate system. This implies that the equations of the thermoelastic problem have to be written first in the material coordinate system and then in the laminate one. The constitutive equations of thermoelasticity can be derived from the Helmholtz free-energy function as in Reddy [33]. Even if all the material data are given in the material reference system, taking into account possible rotations of the fiber direction, the constitutive relation can be rewritten in the laminate reference system as:

$$\boldsymbol{\sigma}^k = \boldsymbol{C}^k \varepsilon^k - \boldsymbol{\lambda}^k \theta^k \tag{1}$$

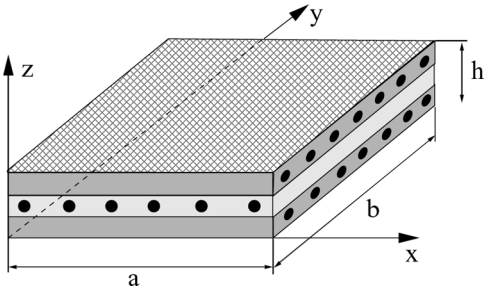

Figure 1 Geometry and notation for multilayered plates.

where $\boldsymbol{\sigma}^k$ is the vector of the stresses, $\boldsymbol{C}^k$ is the matrix of the elastic moduli, ε^k is the vector of the strains, $\boldsymbol{\lambda}^k$ is the vector of the stress-temperature coefficients, θ^k is the variation in temperature with respect to the reference at which stresses and strains temperature do not exist, and the superscript k indicates the affiliation of the relative quantity to the k-th lamina.

Using Voigt's contracted single-subscript notation Equation (1) can be written as:

$$\begin{bmatrix}\sigma_1\\ \sigma_2\\ \sigma_3\\ \sigma_4\\ \sigma_5\\ \sigma_6\end{bmatrix}^k = \begin{bmatrix}C_{11} & C_{12} & C_{13} & 0 & 0 & C_{16}\\ C_{12} & C_{22} & C_{23} & 0 & 0 & C_{26}\\ C_{13} & C_{23} & C_{33} & 0 & 0 & C_{36}\\ 0 & 0 & 0 & C_{44} & C_{45} & 0\\ 0 & 0 & 0 & C_{45} & C_{55} & 0\\ C_{16} & C_{26} & C_{36} & 0 & 0 & C_{66}\end{bmatrix}^k \begin{bmatrix}\varepsilon_1\\ \varepsilon_2\\ \varepsilon_3\\ \varepsilon_4\\ \varepsilon_5\\ \varepsilon_6\end{bmatrix}^k - \begin{bmatrix}\lambda_1\\ \lambda_2\\ \lambda_3\\ \lambda_4\\ \lambda_5\\ \lambda_6\end{bmatrix}^k \theta^k \tag{2}$$

The explicit relations between the material constants in the two reference systems is recalled from Reddy [33] and can be found in the appendix.

From this point forward, stresses and strains will be separated into in-plane and normal components denoted respectively by the subscripts p and n. As a result, the Hooke relation can be written as:

$$\begin{aligned}\boldsymbol{\sigma}^k_{pH} = \begin{bmatrix}\sigma_{1H}\\ \sigma_{2H}\\ \sigma_{6H}\end{bmatrix}^k &= \begin{bmatrix}C_{11} & C_{12} & C_{16}\\ C_{12} & C_{22} & C_{26}\\ C_{16} & C_{26} & C_{66}\end{bmatrix}^k \begin{bmatrix}\varepsilon_1\\ \varepsilon_2\\ \varepsilon_6\end{bmatrix}^k + \begin{bmatrix}0 & 0 & C_{13}\\ 0 & 0 & C_{23}\\ 0 & 0 & C_{36}\end{bmatrix}^k \begin{bmatrix}\varepsilon_5\\ \varepsilon_4\\ \varepsilon_3\end{bmatrix}^k\\ &= \boldsymbol{C}^k_{pp}\varepsilon^k_p + \boldsymbol{C}^k_{pn}\varepsilon^k_n\end{aligned} \tag{3}$$

$$\begin{aligned}\boldsymbol{\sigma}^k_{nH} = \begin{bmatrix}\sigma_{5H}\\ \sigma_{4H}\\ \sigma_{3H}\end{bmatrix}^k &= \begin{bmatrix}0 & 0 & 0\\ 0 & 0 & 0\\ C_{13} & C_{23} & C_{36}\end{bmatrix}^k \begin{bmatrix}\varepsilon_1\\ \varepsilon_2\\ \varepsilon_6\end{bmatrix}^k + \begin{bmatrix}C_{55} & C_{45} & 0\\ C_{45} & C_{44} & 0\\ 0 & 0 & C_{33}\end{bmatrix}^k \begin{bmatrix}\varepsilon_5\\ \varepsilon_4\\ \varepsilon_3\end{bmatrix}^k\\ &= \boldsymbol{C}^{kT}_{pn}\varepsilon^k_p + \boldsymbol{C}^k_{nn}\varepsilon^k_n\end{aligned} \tag{4}$$

Similarly, thermal stresses are split into:

$$\boldsymbol{\sigma}_{pT}^{k} = \begin{bmatrix} \sigma_{1T} \\ \sigma_{2T} \\ \sigma_{6T} \end{bmatrix}^{k} = \begin{bmatrix} \lambda_1 \\ \lambda_2 \\ \lambda_6 \end{bmatrix}^{k} \theta^k = \boldsymbol{\lambda}_p^k \theta^k \tag{5}$$

$$\boldsymbol{\sigma}_{nT}^{k} = \begin{bmatrix} \sigma_{5T} \\ \sigma_{4T} \\ \sigma_{3T} \end{bmatrix}^{k} = \begin{bmatrix} \lambda_5 \\ \lambda_4 \\ \lambda_3 \end{bmatrix}^{k} \theta^k = \boldsymbol{\lambda}_n^k \theta^k \tag{6}$$

where $\boldsymbol{\lambda}_5 = \boldsymbol{\lambda}_4 = 0$ for an orthotropic material.

Mechanical strains can be related to the displacement field $\boldsymbol{u}^k = \left\{ u_x^k,\ u_y^k,\ u_z^k \right\}$ via the geometric relations:

$$\varepsilon_p^k = \boldsymbol{D}_p \boldsymbol{u}^k \tag{7}$$

$$\varepsilon_n^k = (\boldsymbol{D}_{np} + \boldsymbol{D}_{nz}) \boldsymbol{u}^k \tag{8}$$

wherein the differential operator arrays are defined as follows:

$$\boldsymbol{D}_p = \begin{bmatrix} \partial_x & 0 & 0 \\ 0 & \partial_y & 0 \\ \partial_y & \partial_x & 0 \end{bmatrix} \quad \boldsymbol{D}_{np} = \begin{bmatrix} 0 & 0 & \partial_x \\ 0 & 0 & \partial_y \\ 0 & 0 & 0 \end{bmatrix} \quad \boldsymbol{D}_{nz} = \begin{bmatrix} \partial_z & 0 & 0 \\ 0 & \partial_z & 0 \\ 0 & 0 & \partial_z \end{bmatrix} \tag{9}$$

UNIFIED FORMULATION FOR DISPLACEMENTS AND TEMPERATURE

Since the proposed formulation is based on the classical PVD, the only unknown of the problem is the displacement field $\boldsymbol{u}^k$. In the framework of the unified formulation introduced by Carrera [30], the unknowns are assumed by using a generalized expansion that permits one to develop both equivalent single layer and layer-wise analyses:

$$\boldsymbol{u}(x,y,z) = F_b^u(z)\boldsymbol{u}_b(x,y) + F_r^u(z)\boldsymbol{u}_r(x,y) + F_t^u(z)\boldsymbol{u}_t(x,y) = F_r^u \boldsymbol{u}_\tau \tag{10}$$

where N is the order of the expansion and F_τ are called thickness functions and depend only on z.

Equivalent Single-Layer Displacements Formulation

If an equivalent single layer theory is addressed, the thickness functions F_τ take the form

$$F_b = 1, \quad F_r = z^r, \quad F_t = z^N \quad r = 1, 2, \ldots, N-1 \tag{11}$$

In this case the ZZ form of the displacements can be reproduced by referring to Murakami's idea [19] and the displacement model can be written in the following

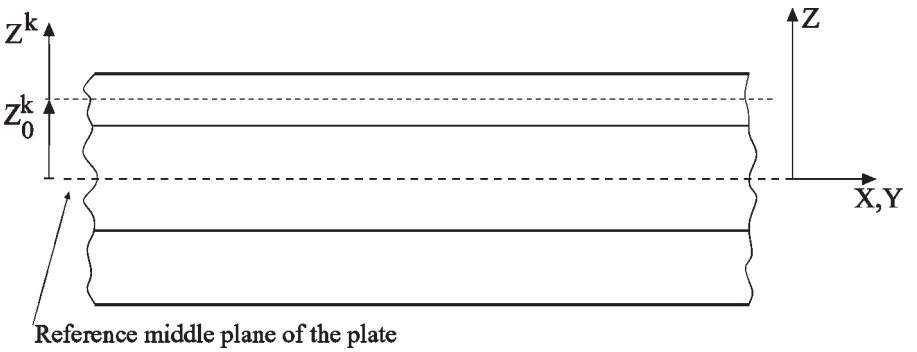

Figure 2 Thickness coordinates for multilayered plates.

generalized form:

$$\boldsymbol{u} = \boldsymbol{u}_0 + (-1)^k \zeta_k \boldsymbol{u}_\zeta + z^r \boldsymbol{u}_r \quad r = 1, 2, \ldots, N; \;\; k = 1, \ldots, N_L \tag{12}$$

where $\zeta_k = 2z_k/h_k$ (see Figure 2) is a non dimensional layer coordinate (z_k is the physical coordinate of the k-layer whose thickness is h_k) and N_L is the total number of layers. The same idea has been used by Ali et al. [25] for his higher-order theory. In generalized form Equation (12) can be written as in Equation (10), after defining the thickness functions as:

$$F_b = 1, \quad F_t = P_z(z) = (-1)^k \zeta_k, \quad F_r = z^r \quad r = 1, 2, \ldots, N \tag{13}$$

Layer-Wise Displacements Formulation

In a layer-wise theory the thickness functions are defined by:

$$F_t = \frac{P_0 + P_1}{2}, \quad F_b = \frac{P_0 - P_1}{2}, \quad F_r = P_r - P_{r-2} \quad r = 2, \ldots, N \tag{14}$$

where $P_i = P_i(\zeta_k)$ is the Legendre polynomial of i-th order defined in the domain $-1 \leq \zeta_k \leq 1$. The chosen thickness functions have the interesting properties:

$$\zeta_k = \begin{cases} 1: \;\; F_t = 1, & F_b = 0, \quad F_r = 0 \\ -1: \;\; F_t = 0, & F_b = 1, \quad F_r = 0 \end{cases} \tag{15}$$

Using these definitions, the generalized displacements representation for the k-th layer can be stated as:

$$\begin{aligned} \boldsymbol{u}^k(x, y, z) &= F_b(z)\boldsymbol{u}_b^k(x, y) + F_r(z)\boldsymbol{u}_r^k(x, y) + F_t(z)\boldsymbol{u}_t^k(x, y) = F_\tau \boldsymbol{u}_\tau^k \\ &\text{with } r = 2, \ldots, N; \;\; k = 1, 2, \ldots, N_L \end{aligned} \tag{16}$$

Thus, the displacement variables $\boldsymbol{u}_b$ and $\boldsymbol{u}_t$ are the actual displacements at the bottom and the top surfaces of the layer and the inter-laminar continuity conditions

can be easily expressed:

$$\boldsymbol{u}_t^k = \boldsymbol{u}_b^{(k+1)}, \quad \text{with } k = 1, \ldots, N_L - 1 \tag{17}$$

Temperature Formulation

Regarding the temperature field, using the same representation as for the displacement quantities but due to the fact that thermal properties of the material can be different in each layer and to the IC condition:

$$\theta_t^k = \theta_b^{(k+1)}, \quad k = 1, \ldots, N_L - 1 \tag{18}$$

Only LW expansion will be used:

$$\begin{aligned} \theta^k &= F_t^\theta \theta_t^k + F_b^\theta \theta_b^k + F_r^\theta \theta_r^k = F_\tau^\theta \theta_\tau^k \\ &\text{where } r = 2, \ldots, N; \;\; k = 1, 2, \ldots, N_L \end{aligned} \tag{19}$$

The actual distribution of the temperature through the plate thickness can be obtained by solving the heat conduction equation as in Tungikar and Rao [26]. For the case of laminates, it has been shown that the temperature distribution $\theta(z)$ is of C_z^0 type, so it could be easily handled by Equation (19). However, in this work, only a simple linear antisymmetric variation is considered because of its capability to bring out important nonclassical influences such as transverse shear deformation and thickness strains.

Even if theoretically the order of the expansion of the displacement field and that of the temperature are independent, for the sake of simplicity the same order has been assumed.

Acronym Explanation

The most important aspect of the unified formulation is that using a special assembling procedure, the number of nodes of the element, the order of the expansion, and the description of the unknowns can be taken as parameters of the performed analysis. In so doing, different numbers of nodes per elements and different theories can be tested using the same formulation. In the present work, the number of nodes per element has been limited to four and nine and the order of the expansion can be chosen from one to four. To quickly address the performed analyses, an acronym has been introduced. Figure 3 explains how the acronym is built. For instance, LD3 is a third-order layer-wise theory based on the PVD; ED2 is a parabolic equivalent single-layer one; EDZ1 is obtained by adding the Murakami ZZ function to ED1 case.

FINITE ELEMENT DISCRETIZATION

In the finite element method the unknowns are expressed in terms of their nodal values, via the shape functions N_i:

$$\boldsymbol{u}_\tau^k(x, y) = N_i \boldsymbol{q}_{\tau i}^k \quad i = 1, 2, \ldots, N_n \tag{20}$$

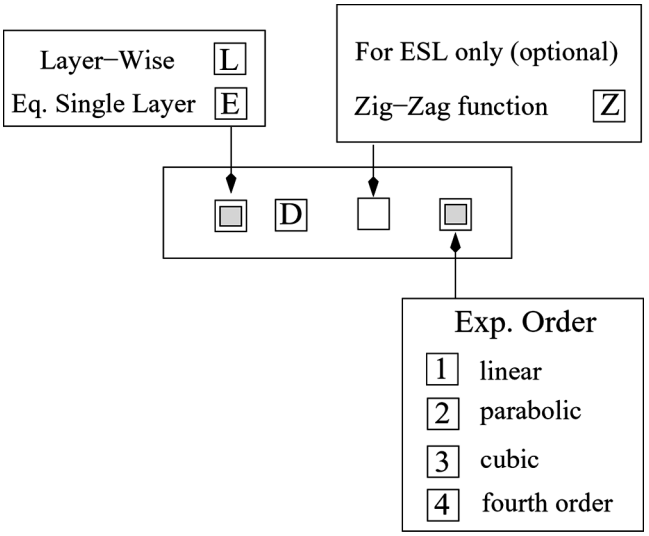

Figure 3 Explanation of the analysis acronym.

where N_n denotes the number of nodes of the element, while:

$$\boldsymbol{q}_{\tau i}^{k} = \begin{bmatrix} q_{u_x \tau i}^{k} \\ q_{u_y \tau i}^{k} \\ q_{u_z \tau i}^{k} \end{bmatrix} \tag{21}$$

Substituting Equation (20) in Equation (10) or Equation (16), the final expression of the displacement field can be obtained:

$$\boldsymbol{u}^{k}(x, y, z) = F_{\tau}^{u} N_i \boldsymbol{q}_{\tau i}^{k} \tag{22}$$

Since the temperature is taken into account as if it was an external load, the generic function $\theta_{\tau}^{k}(x, y)$ can be written:

$$\theta_{\tau}^{k}(x, y) = t(x, y) A_{\tau}^{k} \tag{23}$$

where t takes into account the in-plane shape of the imposed temperature. Now expressing A_{τ}^{k} in terms of the nodal values of the temperature via the shape functions:

$$A_{\tau}^{k} = N_i a_{\tau i}^{k} \quad i = 1, 2, \ldots, N_n \tag{24}$$

and putting together Equations (19), (24), and (23), the temperature discretization takes the form:

$$\theta^{k}(x, y, z) = F_{\tau}^{\theta} t N_i a_{\tau i}^{k} \tag{25}$$

In our formulation classical Lagrange quadrangular elements are considered, and the number of nodes are indicated respectively by Q4 and Q9.

DERIVATION OF THE FINITE ELEMENT MODEL AND FUNDAMENTAL NUCLEI

For the whole laminate of N_L layers, the principle of virtual displacement for thermoelastic analysis, considering only applied thermal loads, is formulated as:

$$\sum_{k=1}^{N_L} \int_{A_k} \int_{h_k} \left\{ \delta\varepsilon_p^{k^T} \left(\boldsymbol{\sigma}_{pH}^k - \boldsymbol{\sigma}_{pT}^k \right) + \delta\varepsilon_n^{k^T} \left(\boldsymbol{\sigma}_{nH}^k - \boldsymbol{\sigma}_{nT}^k \right) \right\} dA_k dz = 0 \tag{26}$$

where the integration domains A_k and h_k indicate respectively the reference plane of the lamina and its thickness. One of the most remarkable aspects of the unified formulation is the possibility of building all the finite element matrices involved in the thermoelastic analysis of multilayered plates from simpler arrays called the fundamental nuclei. These arrays have, in the most general case, $[3 \times 3]$ dimension and should therefore be assembled in the convenient way depending on the used variable description. The procedure for obtaining such arrays starts substituting the stresses Equations (3), (4), (5), and (6) and the geometrical relations (7) and (8) into Equation (26) obtaining for the k-th layer:

$$\begin{aligned} \int_{A_k} \int_{h_k} \Big\{ & \left(\boldsymbol{D}_p \delta \boldsymbol{u}^k \right)^T \left[\left(\boldsymbol{C}_{pp}^k \boldsymbol{D}_p + \boldsymbol{C}_{pn}^k (\boldsymbol{D}_{np} + \boldsymbol{D}_{nz}) \right) \boldsymbol{u}^k - \boldsymbol{\lambda}_p^k \theta^k \right] \\ & + \left((\boldsymbol{D}_{np} + \boldsymbol{D}_{nz}) \delta \boldsymbol{u}^k \right)^T \left[\left(\boldsymbol{C}_{pn}^{k^T} \boldsymbol{D}_p + \boldsymbol{C}_{nn}^k (\boldsymbol{D}_{np} + \boldsymbol{D}_{nz}) \right) \boldsymbol{u}^k - \lambda_n^k \theta^k \right] \Big\} dA_k dz = 0 \end{aligned} \tag{27}$$

At this point, introducing Equations (22) and (25), the previous equation can be discretized as:

$$\begin{aligned} \int_{A_k} \int_{h_k} \Big\{ & \left[(\boldsymbol{D}_p) \left(F_\tau^u N_i \delta \boldsymbol{q}_{\tau i}^k \right) \right]^T \left[\left(\boldsymbol{C}_{pp}^k \boldsymbol{D}_p + \boldsymbol{C}_{pn}^k (\boldsymbol{D}_{np} + \boldsymbol{D}_{nz}) \right) \left(F_s^u N_j \boldsymbol{q}_{sj}^k \right) - \boldsymbol{\lambda}_p^k \left(F_s^\theta t N_j a_{sj}^k \right) \right] \\ & + \left[(\boldsymbol{D}_{np} + \boldsymbol{D}_{nz}) \left(F_\tau^u N_i \delta \boldsymbol{q}_{\tau i}^k \right) \right]^T \left[\left(\boldsymbol{C}_{pn}^k \boldsymbol{D}_p + \boldsymbol{C}_{nn}^k (\boldsymbol{D}_{np} + D_{nz}) \right) \left(F_s^u N_j \boldsymbol{q}_{sj}^k \right) \right. \\ & \left. - \boldsymbol{\lambda}_n^k \left(F_s^\theta t N_j a_{sj}^k \right) \right] \Big\} dA_k dz = 0 \end{aligned} \tag{28}$$

where the superscripts u and θ on the thickness functions indicate the affiliation of a quantity to the displacements and temperature respectively.

In the attempt to make the coefficient of thermal expansion of each layer appear in the fundamental nucleus linked to temperature, the stress-temperature coefficients are rewritten as:

$$\boldsymbol{\lambda}_p^k = \begin{bmatrix} \lambda_1 \\ \lambda_2 \\ \lambda_6 \end{bmatrix}^k = \boldsymbol{\lambda}_{pp}^k + \boldsymbol{\lambda}_{pn}^k \tag{29}$$

$$\boldsymbol{\lambda}_n^k = \begin{bmatrix} 0 \\ 0 \\ \lambda_3 \end{bmatrix}^k = \boldsymbol{\lambda}_{np}^k + \boldsymbol{\lambda}_{nn}^k \tag{30}$$

where

$$\boldsymbol{\lambda}_{pp}^{k} = \boldsymbol{C}_{pp}^{k}\boldsymbol{\alpha}_{p}^{k} \quad \boldsymbol{\lambda}_{pn}^{k} = \boldsymbol{C}_{pn}^{k}\boldsymbol{\alpha}_{n}^{k} \tag{31}$$

$$\boldsymbol{\lambda}_{np}^{k} = \boldsymbol{C}_{pn}^{k^T}\boldsymbol{\alpha}_{p}^{k} \quad \boldsymbol{\lambda}_{nn}^{k} = \boldsymbol{C}_{nn}^{k}\boldsymbol{\alpha}_{n}^{k} \tag{32}$$

and

$$\boldsymbol{\alpha}_{p}^{k} = \begin{bmatrix} \alpha_1 \\ \alpha_2 \\ \alpha_6 \end{bmatrix}^{k} \quad \boldsymbol{\alpha}_{n}^{k} = \begin{bmatrix} 0 \\ 0 \\ \alpha_3 \end{bmatrix}^{k} \tag{33}$$

are the coefficients of thermal expansion of the k-th lamina in the plate reference system whose explicit expression can be found in the appendix. Separating each term of Equation (28) and defining:

$$\boldsymbol{I} = \begin{bmatrix} 1 & 0 & 0 \\ 0 & 1 & 0 \\ 0 & 0 & 1 \end{bmatrix} \tag{34}$$

we obtain:

$$\begin{aligned}
&\delta\boldsymbol{q}_{\tau i}^{k^T}\int_{A_k}\left(\boldsymbol{D}_p^T N_i\right)\boldsymbol{C}_{pp}^{k}\left[\int_{h_k}F_\tau^u F_s^u dz\right](\boldsymbol{D}_p N_j)dA_k\boldsymbol{q}_{sj}^{k} \\
&+\delta\boldsymbol{q}_{\tau i}^{k^T}\int_{A_k}\left(\boldsymbol{D}_p^T N_i\right)\boldsymbol{C}_{pn}^{k}\left[\int_{h_k}F_\tau^u F_s^u dz\right](\boldsymbol{D}_{np} N_j)dA_k\boldsymbol{q}_{sj}^{k} \\
&+\delta\boldsymbol{q}_{\tau i}^{k^T}\int_{A_k}\left(\boldsymbol{D}_p^T N_i\right)\boldsymbol{C}_{pn}^{k}\left[\int_{h_k}F_\tau^u F_{s,z}^u dz\right](N_j\boldsymbol{I})dA_k\boldsymbol{q}_{sj}^{k} \\
&-\delta\boldsymbol{q}_{\tau i}^{k^T}\int_{A_k}\left(\boldsymbol{D}_p^T N_i\right)(\boldsymbol{C}_{pp}^{k}\alpha_p^k+\boldsymbol{C}_{pn}^{k}\alpha_n^k)\left[\int_{h_k}F_\tau^u F_s^\theta dz\right]t(N_j\boldsymbol{I})dA_k a_{sj}^{k} \\
&+\delta\boldsymbol{q}_{\tau i}^{k^T}\int_{A_k}\left(\boldsymbol{D}_{np}^T N_i\right)\boldsymbol{C}_{pn}^{k^T}\left[\int_{h_k}F_\tau^u F_s^u dz\right](\boldsymbol{D}_p N_j)dA_k\boldsymbol{q}_{sj}^{k} \\
&+\delta\boldsymbol{q}_{\tau i}^{k^T}\int_{A_k}\left(\boldsymbol{D}_{np}^T N_i\right)\boldsymbol{C}_{nn}^{k}\left[\int_{h_k}F_\tau^u F_s^u dz\right](\boldsymbol{D}_{np} N_j)dA_k\boldsymbol{q}_{sj}^{k} \\
&+\delta\boldsymbol{q}_{\tau i}^{k^T}\int_{A_k}\left(\boldsymbol{D}_{np}^T N_i\right)\boldsymbol{C}_{nn}^{k}\left[\int_{h_k}F_\tau^u F_{s,z}^u dz\right](N_j\boldsymbol{I})dA_k\boldsymbol{q}_{sj}^{k} \\
&-\delta\boldsymbol{q}_{\tau i}^{k^T}\int_{A_k}\left(\boldsymbol{D}_{np}^T N_i\right)(\boldsymbol{C}_{pn}^{k^T}\alpha_p^k+\boldsymbol{C}_{nn}^{k}\alpha_n^k)\left[\int_{h_k}F_\tau^u F_s^\theta dz\right]t(N_j\boldsymbol{I})dA_k a_{sj}^{k} \\
&+\delta\boldsymbol{q}_{\tau i}^{k^T}\int_{A_k}(N_i\boldsymbol{I})\boldsymbol{C}_{pn}^{k^T}\left[\int_{h_k}F_{\tau,z}^u F_s^u dz\right](D_p N_j)dA_k\boldsymbol{q}_{sj}^{k} \\
&+\delta\boldsymbol{q}_{\tau i}^{k^T}\int_{A_k}(N_i\boldsymbol{I})\boldsymbol{C}_{nn}^{k}\left[\int_{h_k}F_{\tau,z}^u F_s^u dz\right](D_{np} N_j)dA_k\boldsymbol{q}_{sj}^{k} \\
&+\delta\boldsymbol{q}_{\tau i}^{k^T}\int_{A_k}(N_i\boldsymbol{I})\boldsymbol{C}_{nn}^{k}\left[\int_{h_k}F_{\tau,z}^u F_{s,z}^u dz\right](N_j\boldsymbol{I})dA_k\boldsymbol{q}_{sj}^{k} \\
&-\delta\boldsymbol{q}_{\tau i}^{k^T}\int_{A_k}(N_i\boldsymbol{I})\left(\boldsymbol{C}_{pn}^{k^T}\alpha_p^k+\boldsymbol{C}_{nn}^{k}\alpha_n^k\right)\left[\int_{h_k}F_{\tau,z}^u F_s^\theta dz\right]t(N_j\boldsymbol{I})dA_k a_{sj}^{k}=0
\end{aligned} \tag{35}$$

Now introducing the following notations:

$$\left(E_{\tau s}^{\alpha\beta},\ E_{\tau,zs}^{\alpha\beta},\ E_{\tau s,z}^{\alpha\beta},\ E_{\tau,zs,z}^{\alpha\beta}\right) = \int_{h_k}\left(F_{\tau}^{\alpha}F_{s}^{\beta},\ F_{\tau,z}^{\alpha}F_{s}^{\beta},\ F_{\tau}^{\alpha}F_{s,z}^{\beta},\ F_{\tau,z}^{\alpha}F_{s,z}^{\beta}\right)dz \tag{36}$$

with α and β that can assume the values u, θ, and regrouping conveniently the terms of Equation (5) the following terms can be easily obtained:

$$\begin{aligned}\boldsymbol{K}_{uu}^{k\tau sij} = \int_{A_k}\Big\{&\left(\boldsymbol{D}_p^T N_i\right)\left[\boldsymbol{C}_{pp}^k E_{\tau s}^{uu}\left(\boldsymbol{D}_p N_j\right) + \boldsymbol{C}_{pn}^k E_{\tau s}^{uu}\left(\boldsymbol{D}_{np} N_j\right) + \boldsymbol{C}_{pn}^k E_{\tau s,z}^{uu}\left(N_j I\right)\right]\\ &+\left(\boldsymbol{D}_{np}^T N_i\right)\left[\boldsymbol{C}_{pn}^{kT} E_{\tau s}^{uu}\left(\boldsymbol{D}_p N_j\right) + \boldsymbol{C}_{nn}^k E_{\tau s}^{uu}\left(\boldsymbol{D}_{np} N_j\right) + \boldsymbol{C}_{nn}^k E_{\tau s,z}^{uu}\left(N_j I\right)\right]\\ &+\left(N_i I\right)\left[\boldsymbol{C}_{pn}^{kT} E_{\tau,zs}^{uu}\left(\boldsymbol{D}_p N_j\right) + \boldsymbol{C}_{nn}^k E_{\tau,zs}^{uu}\left(\boldsymbol{D}_{np} N_j\right) + C_{nn}^k E_{\tau,zs,z}^{uu}\left(N_j I\right)\right]\Big\}dA_k\end{aligned} \tag{37}$$

$$\begin{aligned}\boldsymbol{K}_{u\theta}^{k\tau sij} = \int_{A_k}\Big[&\left(\boldsymbol{D}_p^T N_i\right)\left(\boldsymbol{C}_{pp}^k \boldsymbol{\alpha}_p^k + \boldsymbol{C}_{pn}^k \boldsymbol{\alpha}_n^k\right) E_{\tau s}^{u\theta} t\left(N_j I\right) + \left(\boldsymbol{D}_{np}^T N_i\right)\left(\boldsymbol{C}_{pn}^{kT} \boldsymbol{\alpha}_p^k + \boldsymbol{C}_{nn}^k \boldsymbol{\alpha}_n^k\right)\\ &\times E_{\tau s}^{u\theta} t\left(N_j I\right) + \left(N_i I\right)\left(C_{pn}^{kT} \alpha_p^k + C_{nn}^k \alpha_n^k\right) E_{\tau,zs}^{u\theta} t\left(N_j I\right)\Big]dA_k\end{aligned} \tag{38}$$

So that, taking into account the definition of virtual variations, the following governing equations can be written:

$$\delta \boldsymbol{q}_{\tau i}^{kT} : \boldsymbol{K}_{uu}^{k\tau sij} \boldsymbol{q}_{sj}^k = \boldsymbol{K}_{u\theta}^{k\tau sij} a_{sj}^k \tag{39}$$

where $\boldsymbol{K}_{uu}^{k\tau sij}$ and $\boldsymbol{K}_{u\theta}^{k\tau sij}$ are the fundamental nuclei.

Equation (39) is valid for a given set of sub/superscripts ($i,\ j,\ \tau,\ s,\ k$). Finite element matrices are obtained by varying these sub/superscripts over their ranges. C_0^z requirements are enforced at this stage. A detailed description of this procedure has been given by Carrera [31, 32, 36] . Since this procedure does not differ from that of the the purely mechanical case, the procedure was not developed here. The final form of an FE problem of the element/structure is:

$$\boldsymbol{K}\boldsymbol{X} = \boldsymbol{F} \tag{40}$$

where $\boldsymbol{K}$ is the stiffness matrix of the system, $\boldsymbol{X}$ is the vector of the unknown nodal values, and $\boldsymbol{F}$ is the vector of the equivalent nodal values of the external loads (applied temperature only in our case). The fundamental nuclei should be conveniently assembled expanding the indices $i,\ j,\ \tau,\ s$ over their range.

NUMERICAL EVALUATIONS

The derived finite elements have been implemented in a computer code and assessed for various thermal stress problems. Finite element results of the analytical solutions problems that were treated by Bhaskar et al. [24], by Ali, Bhaskar, and Varadan [25], and by Carrera [30] have been reported here. Numerical results are

Table 1 Convergence analysis Q4 element

LD4 Q4 int. type = NI S = 4						
N_e	2×2	4×4	6×6	10×10	20×20	Exact [24]
$\overline{u}\left(0, \frac{b}{2}, \mp\frac{h}{2}\right)$	±16.34 (−9.77%)	±17.64 (−2.60%)	±17.90 (−1.16%)	±18.03 (−0.44%)	±18.12 (+0.01%)	±18.11
$\overline{v}\left(\frac{a}{2}, 0, \mp\frac{h}{2}\right)$	±94.41 (+15.37%)	±84.58 (+3.36%)	±83.01 (+1.44%)	±81.82 (−0.01%)	±81.85 (+0.02%)	±81.83
$\overline{w}\left(\frac{a}{2}, \frac{b}{2}, \pm\frac{h}{2}\right)$	44.57 (+4.40%)	42.97 (+0.66%)	42.79 (+0.23%)	42.70 (+0.02%)	42.72 (+0.07%)	42.69

discussed for the two cases:

1. Cylindrical bending of a plate loaded with a linear through the thickness temperature field given by:

$$\theta = \frac{2\theta_M z}{h} \sin\frac{\pi x}{a}$$

2. Simply supported square plate loaded with a bi-sinusoidal temperature field given by:

$$\theta = \frac{2\theta_M z}{h} \sin\frac{\pi x}{a} \sin\frac{\pi y}{b}$$

where a and b are the dimensions of the plate along x-axis and y-axis respectively, while h is its thickness, and θ_M is the value of the temperature at the top surface of the plate (see Figure 1). Both laminates present three layers and the same stacking sequence [0/90/0]. The layers are made of unidirectional laminae with a thickness of $h_k = h/3$ and their mechanical and thermal properties are:

$$\frac{E_L}{E_T} = 25 \quad \frac{G_{LT}}{E_T} = 0.5 \quad \frac{G_{TT}}{E_T} = 0.2$$

$$\nu_{LT} = \nu_{TT} = 0.25 \quad \frac{\alpha_T}{\alpha_L} = 1125$$

Table 2 Convergence analysis Q9 element

LD4 Q9 int. type = NI S = 4					
N_e	2×2	4×4	6×6	10×10	Exact [24]
$\overline{u}\left(0, \frac{b}{2}, \mp\frac{h}{2}\right)$	±18.74 (+3.48%)	±18.17 (+0.33%)	±18.12 (+0.06%)	±18.11 (+0.00%)	±18.11
$\overline{v}\left(\frac{a}{2}, 0, \mp\frac{h}{2}\right)$	±84.06 (+2.73%)	±82.02 (+0.23%)	±81.90 (+0.09%)	±81.85 (+0.02%)	±81.83
$\overline{w}\left(\frac{a}{2}, \frac{b}{2}, \pm\frac{h}{2}\right)$	43.41 (+1.69%)	42.72 (+0.07%)	42.68 (−0.02%)	42.68 (−0.02%)	42.69

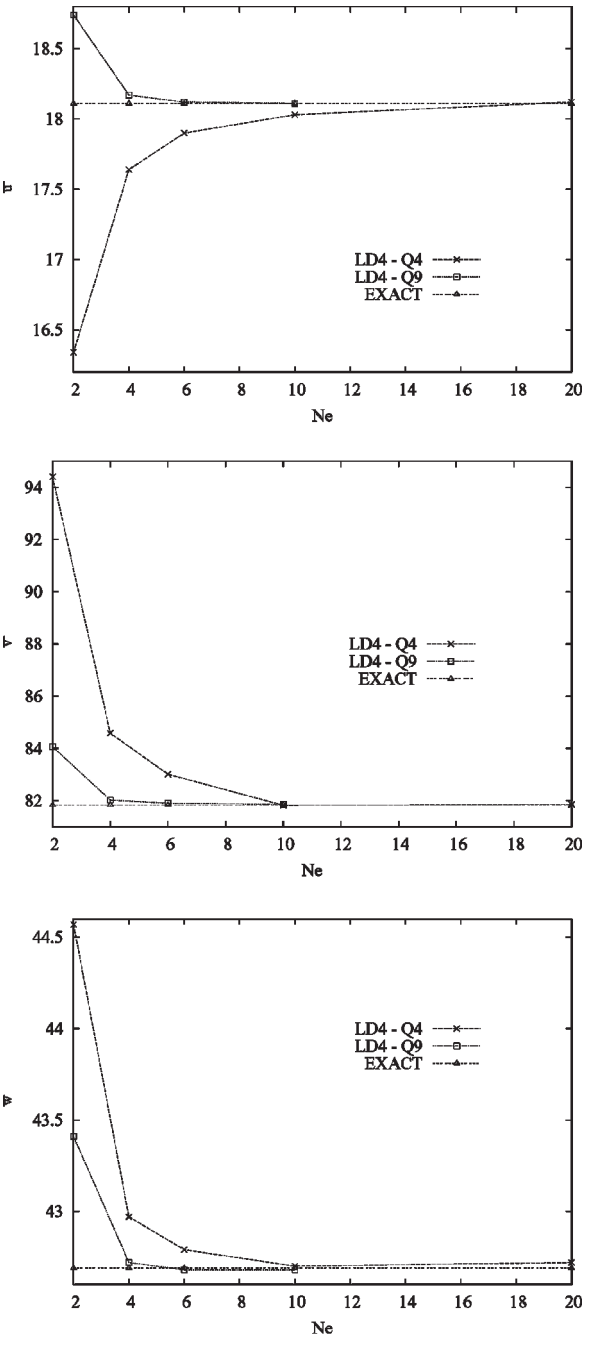

Figure 4 Convergence rate analysis with respect to the number of elements along the plate side N_e; from top to bottom: $\overline{u}\left(0,\ \frac{b}{2},\ \mp\frac{h}{2}\right)$, $\overline{v}\left(\frac{a}{2},\ 0,\ \mp\frac{h}{2}\right)$, $\overline{w}\left(\frac{a}{2},\ \frac{b}{2},\ \pm\frac{h}{2}\right)$.

where E and G are the Young's and shear moduli while the subscripts L and T refer to directions parallel and perpendicular to the fibers. The displacements and stresses at critical in-plane and thickness locations are presented for four different side-to-thickness ratios $S = a/h = 4, 10, 20, 100$. Deflections and stresses are presented in terms of the following dimensionless parameters:

$$\overline{w} = \frac{w}{h\alpha_L\theta_M S^2} \quad (\overline{u},\ \overline{v}) = \frac{(u,\ v)}{h\alpha_L\theta_M S} \quad (\overline{\sigma}_i) = \frac{\sigma_i}{E_T\alpha_L\theta_M S} \tag{41}$$

According to what was done in Carrera et al. [31] the reduced selective integration (SI) has been implemented in order to mitigate the shear locking phenomenon in thin plate cases. However, results are compared to those obtained with the normal Gauss integration (NI). A description of these integration methods applied to FE modeling can be found in Reddy [33] and Hughes [35]. However, the authors are not aware of the fact that more efficient and modern techniques are known to contrast various locking type phenomena. But at the same time most of these techniques have been applied to classical finite element formulations, which are based on FSDT. To the best of the author's knowledge there are not well established, robust, and efficient methods that can contrast the various locking problems that appear in the plate elements derived in this article. Advances on this matter can constitute the subject of future investigations. However, the obtained results will show that the considered thermal stress problem is free from locking mechanisms.

For the simply supported square plate, a convergence analysis to the exact solution [24] of the finite element model has been performed varying the total number of elements and the number of nodes per element for a LD4 formulation and a length-to-thickness ratio of $S = 4$. The results are summarized in Tables 1 and 2 and in Figure 4.

The following comments can be made:

1. Using the same number of elements, the plate element with nine nodes (Q9 element) presents a better convergence ratio than the one with four nodes (Q4 element). The difference between the two elements is considerable, in particular when few elements are used. It can be noted in fact that with the Q9 element only a $[4 \times 4]$ mesh is needed to approximate the exact displacement field with an error less than 0.5%, while the Q4 element needs at least a $[10 \times 10]$ mesh to achieve the same result (the error has been evaluated with respect to 3-D exact solution).
2. The out-of-plane displacement has the best convergence rate for both Q4 and Q9. In the case of a Q9 element with a $[4 \times 4]$ mesh the exact value is approximated with an error around 0.07%.
3. The Q4 element, in general, underestimates the displacement along the x-axis while over-estimates the displacements along the y-axis and z-axis. The Q9 element, instead, tends to overestimate the whole displacement fields.

In the case of the cylindrical bending of a cross-ply plate, such as the one analyzed here, all the field variables are invariant with respect to y-axis.

Table 3 Cases 1: In-plane displacement $\bar{u}\left(0, \frac{b}{2}, \mp\frac{h}{2}\right)$ results

$\bar{u}\left(0, \frac{b}{2}, \mp\frac{h}{2}\right)$ Q9 [6 × 6]				
S	4	10	20	100
Exact [24]	±18.11	±16.61	±16.17	±16.00
Ali et al. [25]	±17.87	±16.59	±16.16	
LD4				
NI	±18.12 (+0.06%)	±16.64 (+0.18%)	±16.20 (+0.19%)	±16.03 (+0.19%)
SI	±18.11 (+0.00%)	±16.64 (+0.18%)	±16.19 (+0.12%)	±16.01 (+0.06%)
A	±18.11 (+0.00%)	±16.61 (+0.00%)	±16.19 (+0.12%)	±16.00 (+0.00%)
LD3				
NI	±18.11 (+0.00%)	±16.64 (+0.18%)	±16.20 (+0.19%)	±16.03 (+0.19%)
SI	±18.11 (+0.00%)	±16.64 (+0.18%)	±16.20 (+0.19%)	±16.01 (+0.06%)
A	±18.10 (+0.00%)	±16.61 (+0.00%)	±16.17 (+0.00%)	±16.00 (+0.00%)
LD2				
NI	±17.73 (−2.10%)	±16.59 (−0.12%)	±16.18 (+0.06%)	±16.03 (+0.19%)
SI	±17.79 (−1.77%)	±16.63 (+0.12%)	±16.20 (+0.19%)	±16.01 (+0.06%)
A	±17.74 (−2.04%)	±16.59 (−0.12%)	±16.16 (−0.06%)	±16.00 (+0.00%)
LD1				
NI	±16.00 (−11.65%)	±16.99 (+2.29%)	±17.04 (+5.39%)	±17.05 (+6.56%)
SI	±16.05 (−11.37%)	±17.03 (+2.53%)	±17.06 (+5.50%)	±17.04 (+6.50%)
A	±16.00 (−11.65%)	±16.98 (+2.23%)	±17.03 (+5.32 %)	±17.03 (+6.44%)
EDZ3				
NI	±17.87 (−1.33%)	±16.61 (+0.00%)	±16.19 (+0.12%)	±16.03 (+0.18%)
SI	±17.92 (−1.32%)	±16.64 (+0.18%)	±16.20 (+0.18%)	±16.01 (+0.06%)
A	±17.87 (−1.33%)	±16.60 (−0.06%)	±16.16 (−0.06%)	±16.00 (+0.00%)
EDZ2				
NI	±14.91 (−17.66%)	±15.94 (−4.03%)	±16.00 (−1.05%)	±16.01 (+0.06%)
SI	±14.96 (−17.39%)	±15.98 (−3.79%)	±16.02 (−0.92%)	±16.00 (+0.00%)
A	±14.92 (−17.61%)	±15.93 (−4.09%)	±15.99 (−1.73%)	±15.99 (−0.06%)
EDZ1				
NI	21.35 (+17.89%)	24.62 (+48.22%)	25.10 (+55.23%)	25.26 (+57.88%)
SI	21.40 (+18.16%)	24.67 (+48.52%)	25.12 (+55.34%)	25.23 (+57.68%)
A	21.35 (+17.89%)	24.62 (+48.22%)	25.07 (+55.04%)	25.21 (+57.56%)
ED4				
NI	±18.20 (+0.50%)	±16.55 (−0.36%)	±16.17 (+0.00%)	±16.03 (+0.19%)
SI	±18.26 (+0.83%)	±16.59 (−0.12%)	±16.18 (+0.06%)	±16.01 (+0.06%)
A	±18.20 (+0.50%)	±16.54 (−0.42%)	±16.14 (−0.19%)	±16.00 (+0.00%)
ED3				
NI	±18.18 (+0.39%)	±16.55 (−0.36%)	±16.17 (+0.00%)	±16.03 (+0.19%)
SI	±18.24 (+0.72%)	±16.59 (−0.12%)	±16.18 (+0.06%)	±16.01 (+0.06%)
A	±18.19 (+0.44%)	±16.54 (−0.42%)	±16.14 (−0.19%)	±15.99 (+0.06%)
ED2				
NI	±10.33 (−42.96%)	±14.66 (−11.74%)	±15.63 (−3.34%)	±15.97 (−0.19%)
SI	±10.36 (−42.79%)	±14.70 (−11.50%)	±15.67 (−3.09%)	±15.99 (−0.06%)
A	±10.35 (−42.85%)	±14.66 (−11.74%)	±15.63 (−3.34%)	±15.98 (−0.13%)
ED1				
NI	±17.02 (−6.02%)	±23.23 (+39.86%)	±24.69 (+52.69%)	±25.20 (+57.50%)
SI	±17.06 (−5.80%)	±23.33 (+40.46%)	±24.75 (+53.06%)	±25.21 (+57.56%)
A	±17.03 (−5.96%)	±23.28 (+40.16%)	±24.70 (+52.75%)	±25.20 (+57.50%)

Errors measured with regards to Bhaskar et al. [24]. Closed-form (A) values are from Carrera [30].

Table 4 Case 1: In-plane displacement $\bar{v}\left(\frac{a}{2}, 0, \mp\frac{h}{2}\right)$ results

$\bar{v}\left(\frac{a}{2}, 0, \mp\frac{h}{2}\right)$ Q9 [6 × 6]				
S	4	10	20	100
Exact [24]	±81.83	±31.95	±20.34	±16.17
Ali et al. [25]	±81.24	±31.92	±20.34	
LD4				
NI	±81.90 (+0.09%)	±32.04 (+0.28%)	±20.47 (+0.64%)	±16.36 (+1.18%)
SI	±81.78 (–0.06%)	±31.89 (–0.19%)	±20.29 (–0.25%)	±16.15 (–0.12%)
A	±81.83 (+0.00%)	±31.95 (+0.00%)	±20.34 (+0.00%)	±16.17 (+0.00%)
LD3				
NI	±81.90 (+0.09%)	±32.04 (+0.28%)	±20.47 (+0.64%)	±16.36 (+1.18%)
SI	±81.76 (–0.09%)	±31.89 (–0.19%)	±20.25 (–0.44%)	±16.15 (–0.12%)
A	±81.82 (–0.01%)	±31.95 (+0.00%)	±20.34 (+0.00%)	±16.17 (+0.00%)
LD2				
NI	±81.22 (–0.75%)	±31.99 (+0.13%)	±20.46 (+0.59%)	±16.36 (+1.18%)
SI	±81.12 (–0.87%)	±31.83 (–0.38%)	±20.24 (–0.49%)	±16.13 (–0.25%)
A	±81.16 (–0.82%)	±31.91 (–0.13%)	±20.34 (+0.00%)	±16.17 (+0.00%)
LD1				
NI	±84.59 (+3.37%)	±33.16 (+3.79%)	±21.50 (+5.70%)	±17.41 (+7.67%)
SI	±84.49 (+3.25%)	±33.00 (+3.29%)	±21.28 (+4.62%)	±17.16 (+6.12%)
A	±84.58 (+3.36%)	±33.12 (+3.66%)	±21.39 (+5.16%)	±17.21 (+6.43%)
EDZ3				
NI	81.31 (–0.63%)	32.00 (+0.15%)	20.46 (+0.58%)	16.36 (+1.17%)
SI	81.20 (–0.76%)	31.83 (–0.37%)	20.24 (–0.49%)	16.13 (–0.24%)
A	81.24 (–0.72%)	31.92 (–0.09%)	20.33 (–0.05%)	16.17 (+0.00%)
EDZ2				
NI	80.87 (–1.17%)	31.45 (–1.56%)	20.28 (–0.29%)	16.35 (+1.11%)
SI	80.76 (–1.30%)	31.30 (–2.03%)	20.06 (–1.38%)	16.12 (–0.31%)
A	80.25 (–1.20%)	31.40 (–1.72%)	20.17 (–0.84%)	16.16 (–0.06%)
EDZ1				
NI	105.7 (+29.17%)	44.75 (+40.06%)	30.69 (+50.88%)	25.74 (+59.18%)
SI	105.6 (+29.04%)	44.55 (+39.44%)	30.39 (+49.41%)	25.39 (+57.02%)
A	105.7 (+29.17%)	44.67 (+39.81%)	30.51 (+50.00%)	25.43 (+57.27%)
ED4				
NI	±76.07 (–7.04%)	±30.28 (–5.23%)	±19.96 (–1.87%)	±16.33 (+0.99%)
SI	±75.93 (–7.21%)	±30.09 (–5.82%)	±19.73 (–3.00%)	±16.11 (–0.37%)
A	±76.04 (–7.08%)	±30.21 (–5.45%)	±19.84 (–2.46%)	±16.15 (–0.12%)
ED3				
NI	±76.06 (–7.05%)	±30.28 (–5.23%)	±19.96 (–1.87%)	±16.33 (+0.99%)
SI	±75.92 (–7.22%)	±30.09 (–5.82%)	±19.73 (–3.00%)	±16.11 (–0.37%)
A	±76.02 (–7.10%)	±30.21 (–5.45%)	±19.84 (–2.46%)	±16.15 (–0.12%)
ED2				
NI	±62.61 (–23.49%)	±26.82 (–16.06%)	±18.98 (–6.69%)	±16.26 (+0.56%)
SI	±62.56 (–23.55%)	±26.82 (–16.06%)	±18.83 (–7.42%)	±16.07 (–0.62%)
A	±64.60 (–21.06%)	±26.89 (–15.84%)	±18.91 (–7.03%)	±16.11 (–0.37%)
ED1				
NI	±88.79 (+8.51%)	±40.29 (+26.10%)	±29.37 (+44.40%)	±25.63 (+58.50%)
SI	±88.73 (+8.43%)	±40.16 (+25.70%)	±29.16 (+43.36%)	±25.35 (+56.77%)
A	±88.71 (+8.41%)	±40.24 (+25.95%)	±29.25 (+43.81%)	±25.37 (+56.90%)

Errors measured with regards to Bhaskar et al. [24]. Closed-form (A) values are from Carrera [30].

Table 5 Case 1: Out of plane displacement $\overline{w}\left(\frac{a}{2},\frac{b}{2},\pm\frac{h}{2}\right)$ results

$\overline{w}\left(\frac{a}{2},\frac{b}{2},\pm\frac{h}{2}\right)$ Q9 [6 × 6]				
S	4	10	20	100
Exact [24]	42.69	17.39	12.12	10.26
Ali et al. [25]	42.34	17.37	12.12	
CLT [30]	10.18 (−76.15%)			10.18 (−0.77%)
LD4				
NI	42.68 (−0.02%)	17.38 (−0.06%)	12.11 (−0.08%)	10.16 (−0.97%)
SI	42.69 (+0.00%)	17.39 (+0.00%)	12.12 (+0.00%)	10.26 (+0.00%)
A	42.69 (+0.00%)	17.39 (+0.00%)	12.12 (+0.00%)	10.26 (+0.00%)
LD3				
NI	42.69 (+0.00%)	17.38 (−0.06%)	12.11 (−0.08%)	10.16 (−0.97%)
SI	42.69 (+0.00%)	17.39 (+0.00%)	12.12 (+0.00%)	10.26 (+0.00%)
A	42.68 (−0.02%)	17.39 (+0.00%)	12.12 (+0.00%)	10.26 (+0.00%)
LD2				
NI	42.25 (−1.03%)	17.36 (−0.17%)	12.10 (−0.17%)	10.16 (−0.97%)
SI	42.25 (−1.03%)	17.37 (−0.12%)	12.12 (+0.00%)	10.26 (+0.00%)
A	42.25 (−1.03%)	17.37 (−0.12%)	12.12 (+0.00%)	10.26 (+0.00%)
LD1				
NI	41.24 (−3.40%)	17.62 (+1.32%)	12.65 (+4.37%)	10.81 (+5.36%)
SI	41.25 (−3.37%)	17.63 (+1.38%)	12.66 (+4.46%)	10.91 (+6.34%)
A	41.24 (−3.40%)	17.63 (+1.38%)	12.66 (+4.46%)	10.93 (+6.53%)
EDZ3				
NI	42.33 (−0.84%)	17.37 (−0.12%)	12.10 (−0.16%)	10.16 (−0.97%)
SI	42.34 (−0.81%)	17.37 (−0.12%)	12.12 (+0.00%)	10.26 (+0.00%)
A	42.33 (−0.84%)	17.37 (−0.12%)	12.12 (+0.00%)	10.26 (+0.00%)
EDZ2				
NI	41.34 (−3.16%)	17.00 (−2.24%)	11.99 (−1.07%)	10.16 (−0.97%)
SI	41.34 (−3.16%)	17.01 (−2.19%)	12.01 (−0.91%)	10.25 (−0.10%)
A	41.34 (−3.16%)	17.01 (−2.19%)	12.01 (−0.91%)	10.26 (+0.00%)
EDZ1				
NI	36.61 (−14.24%)	21.60 (−24.21%)	17.57 (−44.97%)	15.97 (−55.65%)
SI	36.62 (−14.22%)	21.61 (−24.27%)	17.60 (−45.21%)	16.12 (−57.12%)
A	36.61 (−14.24%)	21.61 (−24.27%)	17.60 (−45.21%)	16.12 (−57.12%)
ED4				
NI	42.04 (−1.52%)	16.89 (−2.88%)	11.95 (−1.40%)	10.15 (−1.07%)
SI	42.05 (−1.50%)	16.90 (−2.82%)	11.96 (−1.32%)	10.25 (−0.10%)
A	42.05 (−1.50%)	16.90 (−2.82%)	11.96 (−1.32%)	10.25 (−0.10%)
ED3				
NI	42.04 (−1.52%)	16.89 (−2.88%)	11.95 (−1.40%)	10.15 (−1.07%)
SI	42.05 (−1.50%)	16.90 (−2.82%)	11.96 (−1.32%)	10.25 (−0.10%)
A	42.04 (−1.52%)	16.90 (−2.82%)	11.96 (−1.32%)	10.25 (−0.10%)
ED2				
NI	34.74 (−18.62%)	14.95 (−14.03%)	11.41 (−5.86%)	10.11 (−1.46%)
SI	34.74 (−18.62%)	14.96 (−13.97%)	11.42 (−5.78%)	10.23 (−0.29%)
A	34.74 (−18.62%)	14.96 (−13.97%)	11.42 (−5.78%)	10.23 (−0.29%)
ED1				
NI	30.42 (−28.74%)	19.44 (+11.79%)	16.95 (+39.85%)	15.91 (+55.07%)
SI	30.42 (−28.74%)	19.45 (+11.85%)	16.97 (+40.02%)	16.09 (+56.82%)
A	30.42 (−28.74%)	19.45 (+11.85%)	16.97 (+40.02%)	16.09 (+56.82%)

Errors measured with regards to Bhaskar et al. [24]. Closed-form (A) values are from Carrera [30].

Table 6 Case 2: In-plane displacement $\bar{u}\left(0, y, \mp\frac{h}{2}\right)$ results

$\bar{u}\left(0, \frac{b}{2}, \pm\frac{h}{2}\right)$ Q9 [6 × 1]				
S	4	10	20	100
Exact [24]	±7.470	±5.009	±4.589	±4.449
CLT [30]	±4.444 (–40.50%)	±4.444 (–11.27%)	±4.444 (–3.15%)	±4.444 (–0.11%)
LD4				
NI	±7.478 (+0.11%)	±5.013 (+0.08%)	±4.590 (+0.02%)	±4.460 (+0.25%)
SI	±7.469 (–0.01%)	±5.008 (–0.02%)	±4.588 (–0.02%)	±4.448 (–0.02%)
A	±7.469 (–0.01%)	±5.009 (+0.00%)	±4.589 (+0.00%)	±4.449 (+0.00%)
LD3				
NI	±7.473 (+0.04%)	±5.013 (+0.08%)	±4.589 (+0.00%)	±4.460 (–0.25%)
SI	±7.467 (–0.04%)	±5.009 (+0.00%)	±4.588 (–0.02%)	±4.448 (–0.02%)
A	±7.467 (–0.04%)	±5.009 (+0.00%)	±4.589 (+0.00%)	±4.449 (+0.00%)
LD2				
NI	±7.348 (–1.63%)	±5.005 (–0.08%)	±4.590 (+0.02%)	±4.460 (+0.25%)
SI	±7.344 (–1.69%)	±5.000 (–0.18%)	±4.586 (–0.07%)	±4.448 (–0.02%)
A	±7.345 (–1.67%)	±5.001 (+0.16%)	±4.587 (–0.04%)	±4.449 (+0.00%)
LD1				
NI	±6.137 (–17.84%)	±5.312 (+6.05%)	±5.153 (+12.29%)	±5.101 (+14.65%)
SI	±6.136 (–17.86%)	±5.310 (+6.01%)	±5.147 (+12.16%)	±5.091 (+14.43%)
A	±6.136 (–17.86%)	±5.311 (+6.03%)	±5.147 (+12.16%)	±5.092 (+14.45%)
EDZ3				
NI	±7.494 (+0.32%)	±5.009 (+0.00%)	±4.596 (+0.15%)	±4.460 (+0.25%)
SI	±7.491 (+0.28%)	±5.003 (–0.12%)	±4.587 (–0.04%)	±4.448 (–0.02%)
A	±7.416 (–0.72%)	±5.046 (+0.74%)	±4.588 (–0.02%)	±4.449 (+0.00%)
EDZ2				
NI	±5.316 (–28.84%)	±4.618 (–7.81%)	±4.493 (–2.09%)	±4.453 (+0.09%)
SI	±5.315 (–28.85%)	±4.616 (–7.85%)	±4.488 (–2.20%)	±4.444 (–0.11%)
A	±5.268 (–29.48%)	±4.617 (–7.83%)	±4.489 (–2.18%)	±4.445 (–0.09%)
EDZ1				
NI	±9.890 (+32.40%)	±10.42 (+108.3%)	±10.55 (+129.9%)	±10.60 (+138.2%)
SI	±9.890 (+32.40%)	±10.41 (+107.8%)	±10.54 (+129.6%)	±10.58 (+137.8%)
A	±9.791 (+31.07%)	±10.42 (+108.3%)	±10.54 (+129.6%)	±10.58 (+137.8%)
ED4				
NI	±7.572 (+1.37%)	±5.048 (+0.78%)	±4.606 (+0.37%)	±4.460 (+0.25%)
SI	±7.570 (+1.34%)	±5.044 (+0.70%)	±4.597 (+0.17%)	±4.450 (+0.02%)
A	±7.570 (+1.34%)	±5.044 (+0.70%)	±4.598 (+0.20%)	±4.449 (+0.00%)
ED3				
NI	±7.568 (+1.31%)	±5.048 (+0.78%)	±4.606 (+0.37%)	±4.460 (+0.25%)
SI	±7.566 (+1.29%)	±5.043 (+0.68%)	±4.597 (+0.17%)	±4.450 (+0.02%)
A	±7.566 (+1.29%)	±5.044 (+0.70%)	±4.598 (+0.20%)	±4.450 (+0.02%)
ED2				
NI	±4.465 (–40.23%)	±4.446 (–11.24%)	±4.443 (–3.18%)	±4.442 (–0.16%)
SI	±4.465 (–40.23%)	±4.446 (–11.24%)	±4.443 (–3.18%)	±4.444 (–0.11%)
A	±4.465 (–40.23%)	±4.447 (–11.22%)	±4.445 (–3.14%)	±4.443 (–0.13%)
ED1				
NI	±10.59 (+41.77%)	±10.59 (+111.4%)	±10.58 (+130.5%)	±10.59 (+138.0%)
SI	±10.59 (+41.77%)	±10.59 (+111.4%)	±10.59 (+130.7%)	±10.59 (+138.0%)
A	±10.59 (+41.77%)	±10.59 (+111.4%)	±10.59 (+130.7%)	±10.59 (+138.0%)

Errors measured with regards to Bhaskar et al. [24]. Closed-form (A) values are from Carrera [30].

Table 7 Case 2: out of plane displacement $\overline{\omega}\left(\frac{a}{2}, y, \mp\frac{h}{2}\right)$ results

$\overline{\omega}\left(\frac{a}{2}, \frac{b}{2}, \pm\frac{h}{2}\right)$ Q9 [6 × 1]				
S	4	10	20	100
Exact [24]	18.32	5.408	3.479	2.855
CLT [30]	2.829 (−84.55%)	2.829 (−47.68%)	2.829 (−18.68%)	2.829 (−0.91%)
LD4				
NI	18.37 (+0.27%)	5.409 (+0.02%)	3.476 (−0.09%)	2.830 (−0.88%)
SI	18.37 (+0.27%)	5.410 (+0.04%)	3.478 (−0.03%)	2.855 (+0.00%)
A	18.32 (+0.00%)	5.408 (+0.00%)	3.479 (+0.00%)	2.855 (+0.00%)
LD3				
NI	18.37 (+0.27%)	5.409 (+0.02%)	3.476 (−0.09%)	2.830 (−0.88%)
SI	18.37 (+0.27%)	5.410 (+0.04%)	3.478 (−0.03%)	2.855 (+0.00%)
A	18.32 (+0.00%)	5.408 (+0.00%)	3.479 (+0.00%)	2.855 (+0.00%)
LD2				
NI	18.24 (−0.24%)	5.406 (−0.04%)	3.475 (−0.11%)	2.830 (−0.88%)
SI	18.24 (−0.24%)	5.407 (−0.02%)	3.477 (−0.06%)	2.855 (+0.00%)
A	18.20 (−0.66%)	5.401 (−0.13%)	3.478 (−0.03%)	2.855 (+0.00%)
LD1				
NI	16.14 (−11.90%)	5.386 (−0.41%)	3.776 (+8.54%)	3.233 (+13.24%)
SI	16.14 (−11.90%)	5.387 (−0.39%)	3.779 (+8.62%)	3.262 (+14.26%)
A	16.10 (−12.12%)	5.381 (−0.50%)	3.326 (−4.40%)	3.262 (+14.26%)
EDZ3				
NI	18.27 (−0.27%)	5.404 (−0.07%)	3.475 (−0.11%)	2.830 (−0.88%)
SI	18.27 (−0.27%)	5.405 (−0.06%)	3.478 (−0.03%)	2.854 (−0.04%)
A	18.27 (−0.27%)	5.408 (+0.00%)	3.478 (−0.03%)	2.855 (+0.00%)
EDZ2				
NI	16.98 (−7.31%)	5.160 (−4.59%)	3.412 (−1.93%)	2.827 (−0.98%)
SI	16.98 (−7.31%)	5.161 (−4.57%)	3.415 (−1.84%)	2.852 (−0.11%)
A	16.99 (−7.26%)	5.161 (−4.57%)	3.415 (−1.84%)	2.853 (−0.07%)
EDZ1				
NI	5.581 (−69.54%)	6.491 (+20.03%)	6.668 (+91.66%)	6.676 (+133.8%)
SI	5.580 (−69.54%)	6.493 (+20.06%)	6.674 (+91.84%)	6.736 (+133.9%)
A	5.581 (−69.54%)	6.494 (+20.08%)	6.674 (+91.74%)	6.736 (+133.9%)
ED4				
NI	18.98 (+3.60%)	5.516 (+2.00%)	3.503 (+0.69%)	2.830 (−0.88%)
SI	18.98 (+3.60%)	5.517 (+2.02%)	3.505 (+0.75%)	2.856 (+0.04%)
A	18.98 (+3.60%)	5.517 (+2.02%)	3.505 (+0.75%)	2.856 (+0.04%)
ED3				
NI	18.98 (+3.60%)	5.516 (+2.00%)	3.503 (+0.69%)	2.830 (−0.88%)
SI	18.98 (+3.60%)	5.517 (+2.02%)	3.505 (+0.75%)	2.856 (+0.04%)
A	18.98 (+3.60%)	5.517 (+2.02%)	3.505 (+0.75%)	2.856 (+0.04%)
ED2				
NI	15.81 (−13.70%)	4.912 (−9.17%)	3.347 (−3.79%)	2.818 (−1.30%)
SI	15.81 (−13.70%)	4.913 (−9.15%)	3.350 (−3.71%)	2.849 (−0.21%)
A	15.81 (−13.70%)	4.912 (−9.17%)	3.350 (−3.71%)	2.850 (−0.18%)
ED1				
NI	6.738 (−63.22%)	6.737 (+24.57%)	6.733 (+93.53%)	6.665 (+133.4%)
SI	6.738 (−63.22%)	6.738 (+24.59%)	6.739 (+93.71%)	6.738 (+136.0%)
A	6.739 (−63.22%)	6.739 (+24.61%)	6.739 (+93.71%)	6.739 (+136.0%)

Errors measured with regards to Bhaskar et al. [24]. Closed-form (A) values are from Carrera [30].

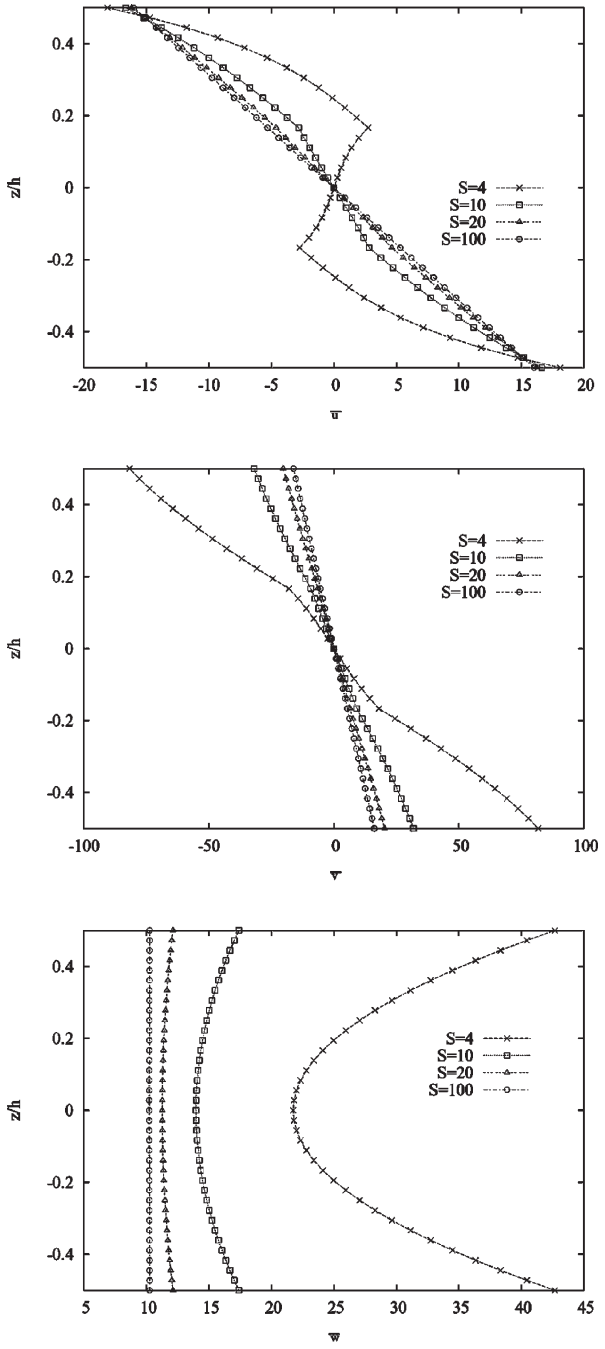

Figure 5 Case 1: Displacement field along the plate thickness for various length-to-thickness ratios using LD4 Q9 element and SI. From top to bottom: $\overline{u}\left(0,\ \frac{b}{2}\right)$, $\overline{v}\left(\frac{a}{2},\ 0\right)$, $\overline{w}\left(\frac{a}{2},\ \frac{b}{2}\right)$.

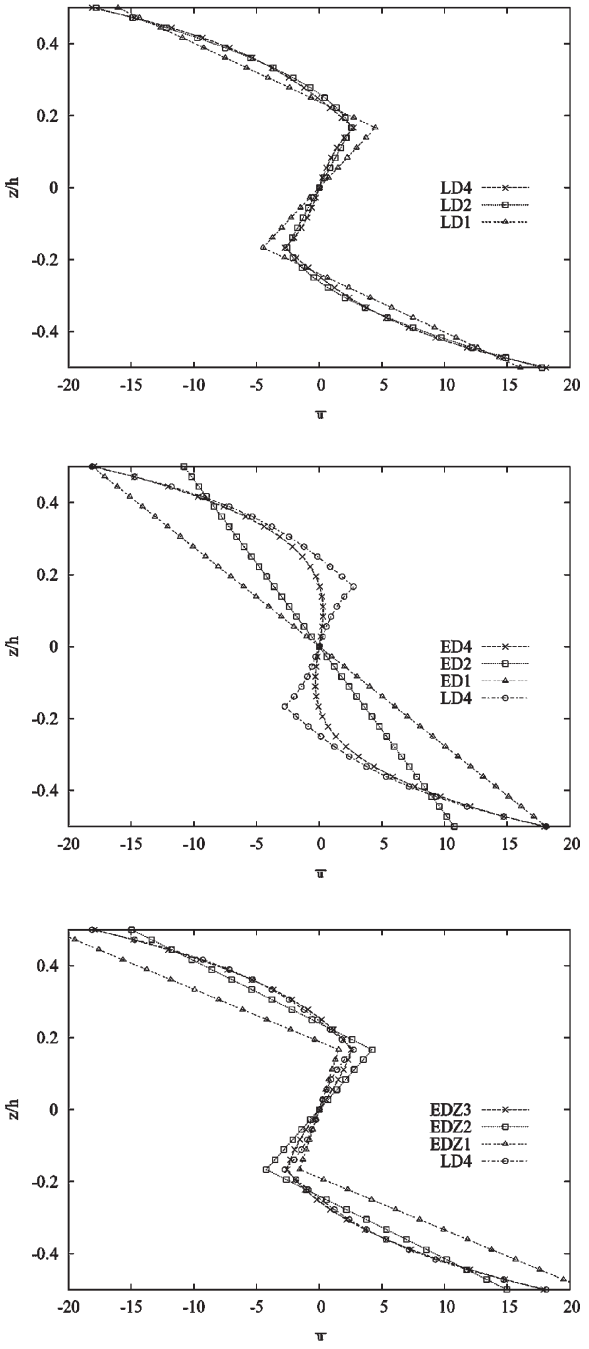

Figure 6 Case 1: Displacement $\overline{u}\left(0,\ \frac{b}{2}\right)$ for various FEs using S = 4, Q9, and SI. From top to bottom: LDs, EDs, EDZs.

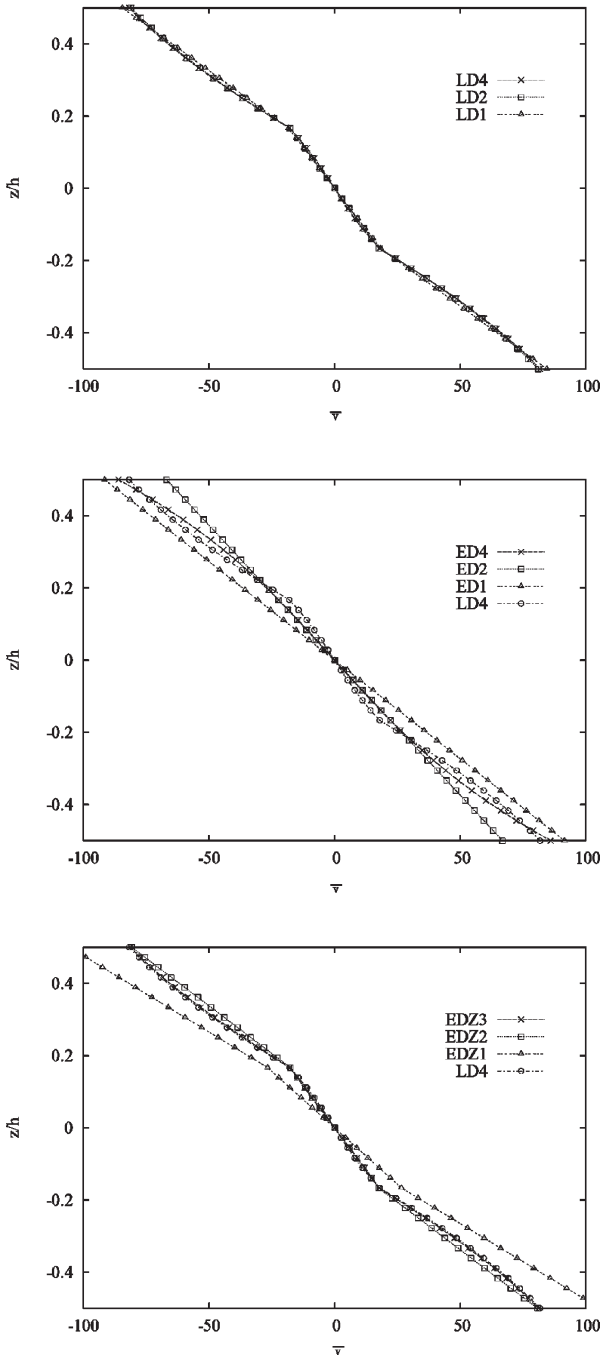

Figure 7 Case 1: Displacement $\bar{v}\left(\frac{a}{2}, 0\right)$ for various FEs using S = 4, Q9, and SI. From top to bottom: LDs, EDs, EDZs.

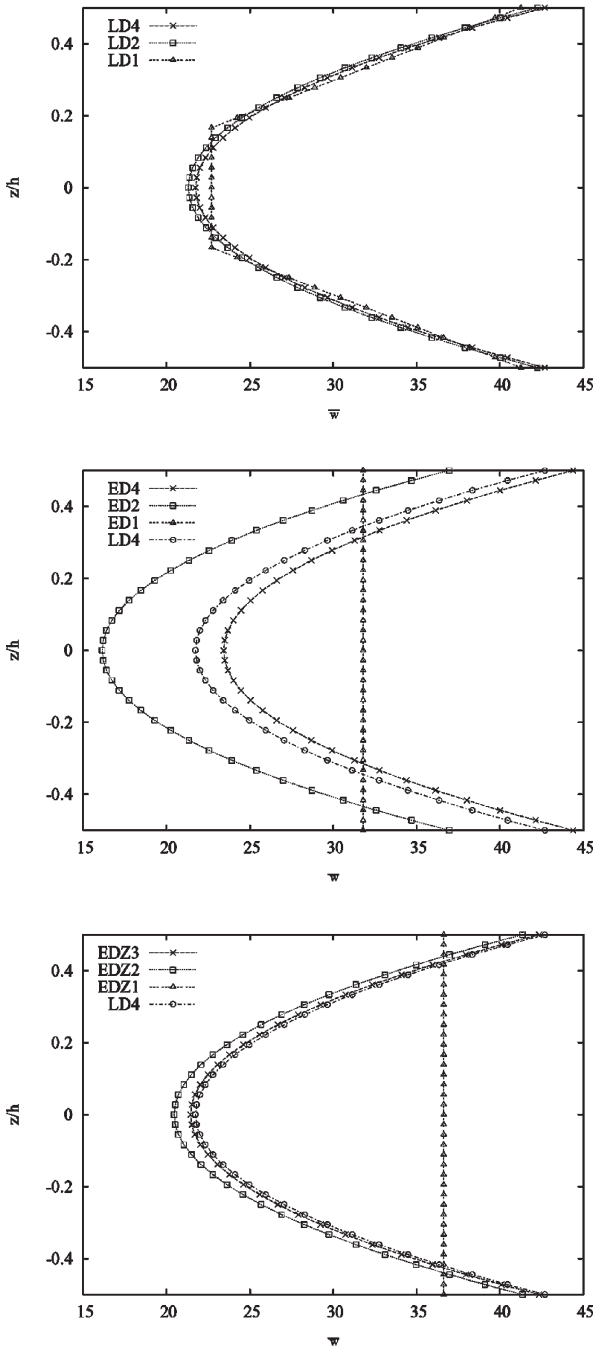

Figure 8 Case 1: Displacement $\overline{w}\left(\frac{a}{2}, \frac{b}{2}\right)$ for various FEs using S = 4, Q9, and SI. From top to bottom: LDs, EDs, EDZs.

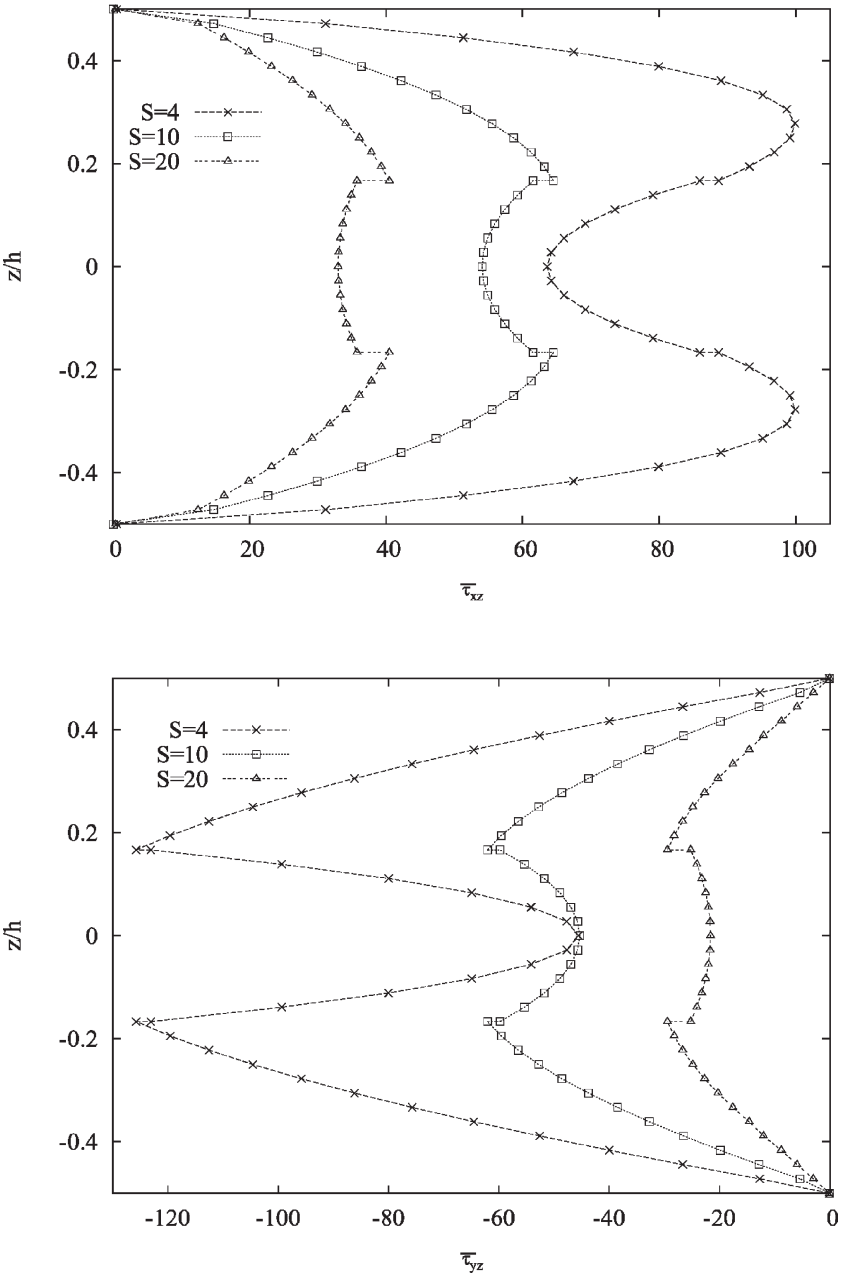

Figure 9 Case 1: Transverse shear stresses distribution for various length-to-thickness ratios using LD4, Q9 FE, and SI. From top to bottom: $\overline{\tau}_{xz}\left(0,\ \frac{b}{2}\right), \overline{\tau}_{yz}\left(\frac{a}{2},\ 0\right)$.

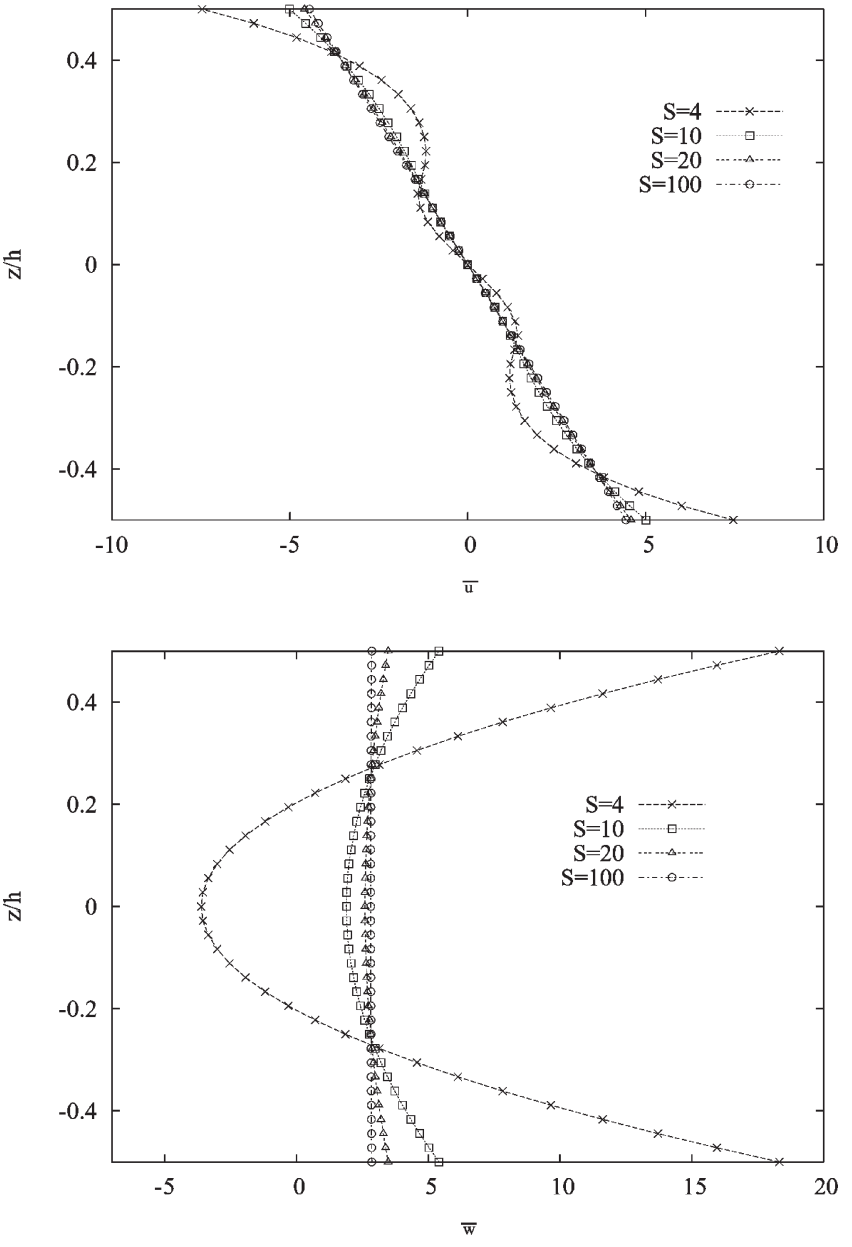

Figure 10 Case 2: From top to bottom: displacement $\overline{u}(0, y)$, displacement $\overline{w}\left(\frac{a}{2}, y\right)$ for various length-to-thickness ratios using LD4 Q9 FE and SI.

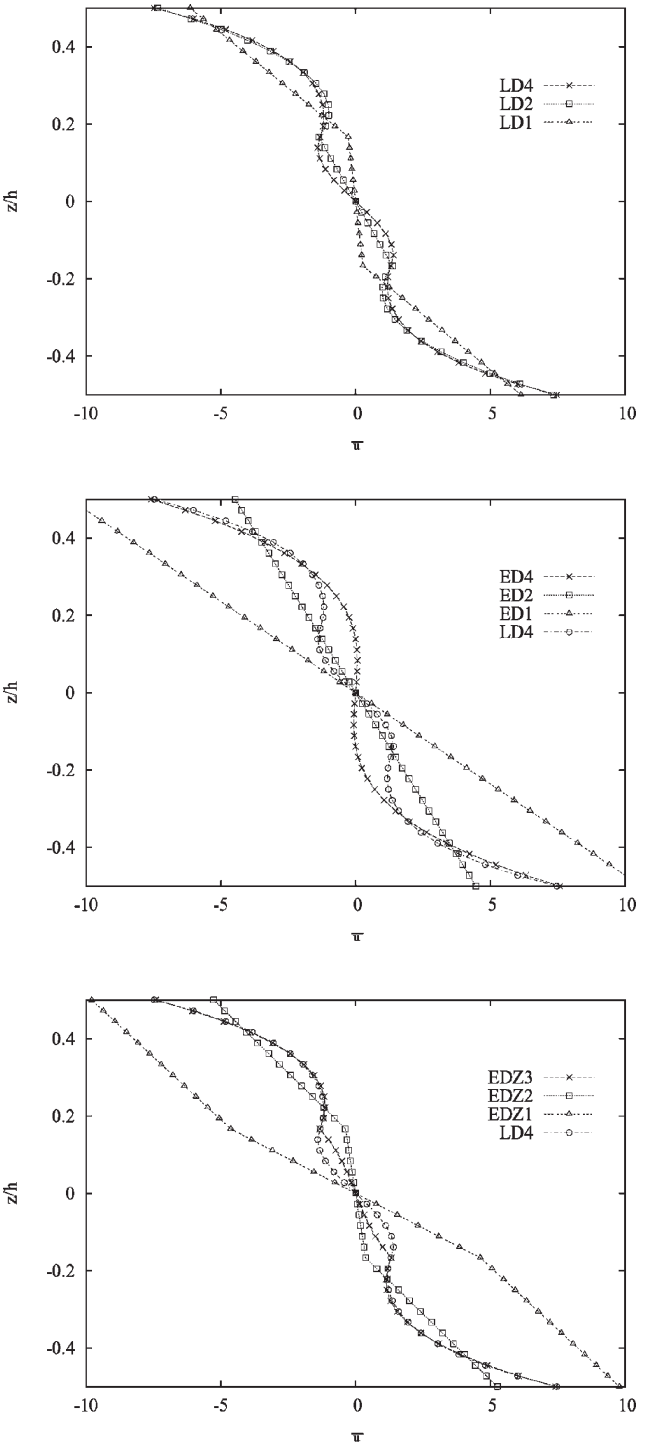

Figure 11 Case 2: Displacement $\overline{u}(0, y)$ for various FEs using S = 4, Q9, and SI. From top to bottom: LDs, EDs, EDZs.

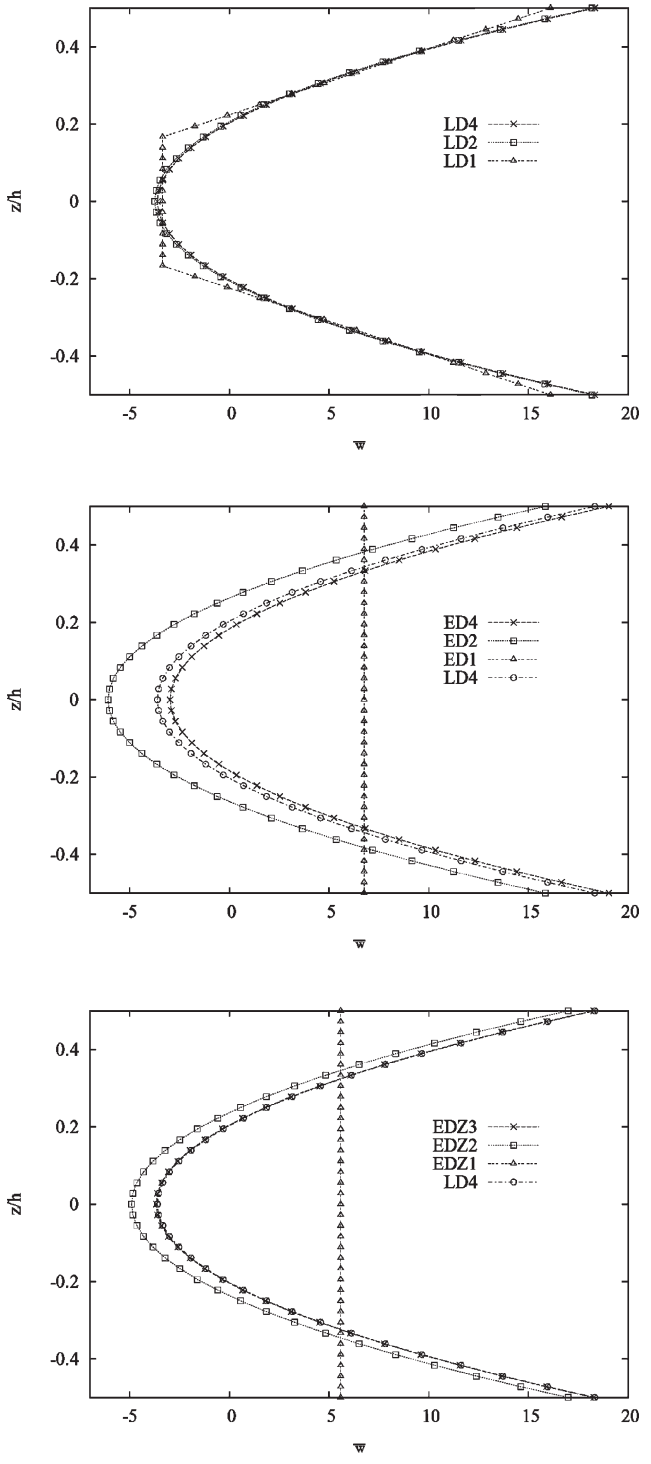

Figure 12 Case 2: Displacement $\overline{w}\left(\frac{a}{2}, y\right)$ for various FEs using S = 4, Q9, and SI. From top to bottom: LDs, EDs, EDZs.

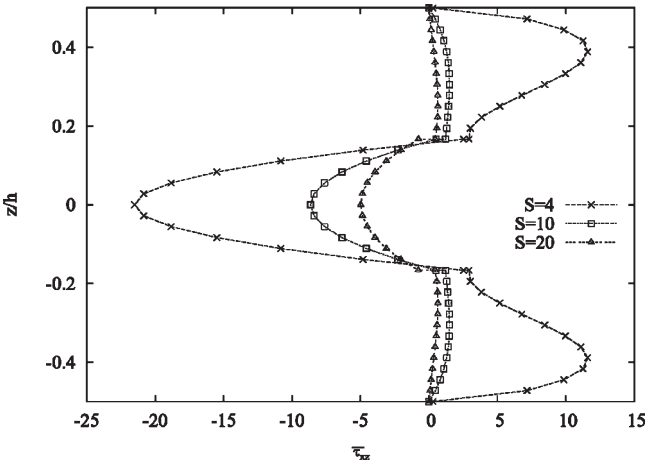

Figure 13 Case 2: Transverse shear stresses distribution $\overline{\tau}_{xz}(0, y)$ for various length-to-thickness ratios using LD4 Q9 FE and SI.

ASSESSMENT OF VARIOUS PLATE ELEMENTS

The displacement fields for different types of analysis and length-to-thickness ratio are listed in Tables 3–5 for the square plate cases. Tables 6 and 7 refer to the cylindrical bending cases. The results are related to the Q9 plate element. The number of elements has been fixed to a $[6 \times 6]$ and a $[6 \times 1]$ mesh respectively for the square plate and the cylindrical bending since these discretizations have shown the best compromise between accuracy (see Table 2) and computational costs. Results for the two different types of integrations have been reported in order to evaluate their effects in thin plate cases. Comparison to analytical (A) closed form exact solutions given in Carrera [30] have been provided. Better numerical performances than those found in the pure mechanical problems treated in Carrera [31] are in general obtained. In fact, NI and SI are very close to the related analytical solution (A) for both thick and thin plates. This means that the considered elements are free from locking mechanisms for the analysis of thermal stress problems. This behavior was not found in Carrera [31], where pure mechanical loadings were considered. However, some benefits are obtained by using SI with respect to NI. In fact, the thinner the plate the bigger the difference between the two integration methods, demonstrating the benefits of selective integration on shear locking.

Related to the comparisons of various FEs, the following comments can be made. In general, layer-wise FEs (LD4-LD1) give better results than equivalent single layer ones (ED4-ED1, EDZ3-EDZ1). The accuracy of the different theories relies on the order of the expansion N. Indeed, LD3 and LD4 match perfectly both the exact solution [24] and the closed-form results of the unified formulation in Carrera [30]. It can be said that equivalent single-layer analyses are quite satisfactory only if applied to thin plates. On the other hand, LD3/4 results are in excellent agreement with 3-D solutions for all the length-to-thickness ratios. In addition, it should be noted that LD type analyses are computationally more expensive.

Table 8 Case 2: In-plane stress $\overline{\sigma_1}\left(\frac{a}{2}, y, \mp\frac{h}{6}\right)$ results

$\overline{\sigma_1}\left(\frac{a}{2}, \frac{b}{2}, \pm\frac{h}{6}\right)$ Q9 [6 × 1]				
S	4	10	20	100
Exact [24]	±372.3	±371.7	±371.5	±371.4
CLT [30]	±371.4 (−0.24%)	±371.4 (−0.08%)	±371.4 (−0.02%)	±371.4 (+0.00%)
LD4				
NI	±372.2 (−0.03%)	±371.5 (−0.05%)	±371.4 (−0.03%)	±371.2 (−0.05%)
SI	±372.1 (−0.05%)	±371.5 (−0.05%)	±371.3 (−0.05%)	±371.3 (−0.03%)
A	±372.3 (+0.00%)	±371.8 (+0.03%)	±371.4 (−0.03%)	±371.3 (−0.03%)
LD3				
NI	±372.4 (+0.03%)	±371.5 (−0.05%)	±371.4 (−0.03%)	±371.2 (−0.05%)
SI	±372.4 (+0.03%)	±371.6 (−0.03%)	±371.3 (−0.05%)	±371.2 (−0.05%)
A	±372.5 (+0.05%)	±371.7 (+0.00%)	±371.4 (−0.03%)	±371.3 (−0.03%)
LD2				
NI	±372.8 (−0.03%)	±371.5 (−0.05%)	±371.4 (−0.08%)	±371.2 (−0.05%)
SI	±372.0 (−0.03%)	±371.5 (−0.05%)	±371.2 (−0.08%)	±371.2 (−0.05%)
A	±372.2 (−0.03%)	±371.8 (+0.03%)	±371.4 (−0.03%)	±371.3 (−0.03%)
LD1				
NI	±502.5 (+34.97%)	±498.6 (+34.14%)	±497.8 (+34.00%)	±497.7 (+34.01%)
SI	±502.5 (+34.97%)	±498.6 (+34.14%)	±497.9 (+34.02%)	±497.6 (+33.98%)
A	±502.3 (+34.91%)	±498.7 (+34.17%)	±498.0 (+34.05%)	±497.7 (+34.01%)
EDZ3				
NI	±371.9 (−0.11%)	±371.6 (−0.03%)	±371.3 (−0.05%)	±371.3 (−0.03%)
SI	±371.9 (−0.11%)	±371.6 (−0.03%)	±371.3 (−0.05%)	±371.2 (−0.05%)
A	±372.0 (−0.08%)	±371.8 (+0.03%)	±371.5 (+0.00%)	±371.4 (+0.00%)
EDZ2				
NI	±375.4 (+0.83%)	±372.1 (+0.11%)	±371.4 (−0.03%)	±371.3 (−0.03%)
SI	±375.4 (+0.83%)	±372.1 (+0.11%)	±371.4 (−0.03%)	±371.2 (−0.05%)
A	±372.3 (+0.00%)	±371.7 (+0.00%)	±371.5 (+0.00%)	±371.4 (+0.00%)
EDZ1				
NI	±487.5 (+30.94%)	±490.5 (+31.96%)	±491.0 (+32.17%)	±491.4 (+32.31%)
SI	±487.5 (+30.94%)	±490.5 (+31.96%)	±491.1 (+32.19%)	±491.3 (+32.28%)
A	±487.9 (+31.05%)	±490.8 (+32.04%)	±491.4 (+32.27%)	±491.6 (+32.36%)
ED4				
NI	±375.9 (+0.97%)	±372.1 (+0.11%)	±371.4 (−0.03%)	±371.3 (−0.03%)
SI	±375.9 (+0.97%)	±372.1 (+0.11%)	371.4 (−0.03%)	371.2 (−0.05%)
A	±376.0 (+0.99%)	±372.3 (+0.16%)	±371.6 (+0.03%)	±371.4 (+0.00%)
ED3				
NI	±376.1 (+1.02%)	±372.1 (+0.11%)	±371.4 (−0.03%)	±371.3 (−0.03%)
SI	±376.1 (+1.02%)	±372.1 (+0.11%)	±371.5 (+0.00%)	±371.2 (−0.05%)
A	±376.2 (+1.05%)	±372.3 (+0.16%)	±371.7 (+0.05%)	±371.5 (+0.03%)
ED2				
NI	±371.7 (−0.16%)	±371.3 (−0.11%)	±371.2 (−0.08%)	±371.4 (+0.00%)
SI	±371.7 (−0.16%)	±371.3 (−0.11%)	±371.2 (−0.08%)	±371.2 (−0.03%)
A	±371.9 (−0.11%)	±371.5 (−0.05%)	±371.5 (+0.00%)	±371.4 (+0.00%)
ED1				
NI	±491.3 (+31.96%)	±491.4 (+32.20%)	±491.4 (+32.27%)	±491.7 (+32.39%)
SI	±491.3 (+31.96%)	±491.3 (+32.18%)	491.3 (+32.25%)	±491.3 (+32.28%)
A	±491.6 (+32.04%)	±491.6 (+32.26%)	491.6 (+32.33%)	±491.6 (+32.36%)

Errors measured with regards to Bhaskar et al. [24]. Closed-form (A) values are from Carrera [30].

CLT results have been quoted for some of the conducted investigations. Good results have been also achieved with LD2 FE (related to parabolic displacement field in each layer, with a relative maximum error around 2% for all cases and ratios). Plate elements that present a constant transverse normal strain such as LD1 and ED1 lead to inaccurate results for both thick and thin plates. It is in fact in agreement with what was found in Carrera [30, 37], at least a parabolic expansion for transverse displacements (u_x, u_y, and u_z components) is required to capture the linear thermal strains that are related to a linear through-the-thickness temperature distribution. LD1 (this is related to a linear displacement field in each layer) gives better results than ED1 FEs, but these are still not satisfactory.

Equivalent single layer results can be very much improved by introducing the Murakami's zig-zag function. This is shown in Figures 6–8, 11, and 12. In addition, all the FEs based on a linear displacement field such as LD1s, ED1s, and EDZ1s show better results for thick plates than for thin ones. Comparing ED1 and EDZ1 results, even if EDZ1 overestimates by 19% the displacement at the top and the bottom of the plate, it is able to describe the ZZ shape and is nearer to the LD4 solution than ED1, which presents just a straight line from the top and bottom values. EDZ3 results are satisfactory for all length-to-thickness ratios, while ED3 results are satisfactory only for ratios greater than or equal to 10. In the case of cylindrical bending, it should be noticed that EDZ3 results in Tables 6 and 7 and in Figures 11 and 12 present high accuracy as compared to LD4 FEs. Figures 9 and 13 show the transverse shear stress distributions along the thickness of the plate. These have been computed through the constitutive Equation (1) and are unable to satisfy the IC conditions; in fact, discontinuities are present at layer interfaces. In-plane stresses σ_1 for case 2 are listed in Table 8.

CONCLUSIONS

This article has derived equivalent single layer (ESL) and layer-wise (LW) thermoelastic finite elements based on a unified formulation. Linear up to fourth-order expansions for the displacement variables have been considered. Numerical results have shown that the most accurate FEs match very well the 3-D exact solutions in order to evaluate both displacements and stresses of thin and thick plates. On the other hand, those FEs with lower order displacement fields can exhibit difficulties in tracing the response of a multilayered plate loaded by linear temperature distribution through the plate thickness.

REFERENCES

1. L. Librescu and M. A. Souza, Postbuckling of Geometrically Imperfect Shear-Deformable Flat Panels Under Combined Thermal and Compressive Edge Loadings, *J. Appl. Mech.*, vol. 60, pp. 526–533, 1993.
2. L. Librescu, W. Lin, M. P. Nemeth, and J. H. Starnes, Jr., Vibration of Geometrically Imperfect Panels Subjected to Thermal and Mechanical Loads, *J. Spacecr. Rockets*, vol. 33, no. 2, pp. 285–291, 1996.
3. L. Librescu, W. Lin, M. P. Nemeth, and J. H. Starnes, Jr., Frequency-Load Interaction of Geometrically Imperfect Curved Panels Subjected to Heating, *AIAA J.*, vol. 34, no. 1, pp. 166–177, 1996.

4. L. Librescu and W. Lin, Vibration of Thermomechanically Loaded Flat and Curved Panels Taking into Account Geometric Imperfections and Tangential Edge Restraints, *Int. J. Solids Struct.*, vol. 34, no. 17, pp. 2161–2181, 1997.
5. T. Hause, L. Librescu, and T. F. Johnson, Nonlinear Response of Geometrically Imperfect Flat and Curved Sandwich Panels Subjected to Thermomechanical Loading, *Int. J. Non-Linear Mech.*, vol. 33, no. 6, pp. 1039–1059, 1998.
6. L. Librescu and W. Q. Lin, Nonlinear Response of Laminated Plates and Shells to Thermomechanical Loading: Implications of Violation of Interlaminar Shear Traction Continuity Requirement, *Int. J. Solids Struct.*, vol. 36, no. 27, pp. 4111–4147, 1999.
7. L. Librescu, M. P. Nemeth, J. H. Starnes, Jr., and W. Lin, Nonlinear Response of Flat and Curved Panels to Thermomechanical Loading, *J. Therm. Stress.*, vol. 23, no. 6, pp. 549–582, 2000.
8. E. Carrera and L. Librescu, Large Deflection FEM Analysis of Thermally Loaded Stiffened, Shear Deformable Plates, in *Recent Advances in Solid/Structures and Applications of Metallic Materials*, pp. 141–154, American Society of Mechanical Engineers, New York, 1997.
9. W. H. Pell, Thermal Deflections of Anisotropic Thin Plates, *Appl. Mech. Rev.*, vol. 4, no. 1, pp. 27–44, 1946.
10. Y. Stavsky, Thermoelasticity of Heterogeneous Oleotropic Plates, *J. Eng. Mech. Div.*, vol. 89, pp. 89–105, 1963.
11. C. H. Wu and T. R. Tauchert, Thermoelastic Analysis of Laminated Plates. 1: Symmetric Specially Orthotropic Laminates, *J. Therm. Stress.*, vol. 3, pp. 247–259, 1980.
12. C. H. Wu and T. R. Tauchert, Thermoelastic Analysis of Laminated Plates. 2: Antisymmetric Cross-Ply and Angle-Ply Laminates, *J. Therm. Stress.*, vol. 3, pp. 365–378, 1980.
13. J. N. Reddy and Y. S. Hsu, Effects of Shear Deformation and Anisotropy on the Thermal Bending of Layered Composite Plates, *J. Therm. Stress.*, vol. 3, pp. 475–493, 1980.
14. J. M. Whitney and N. J. Pagano, Shear Deformation in Heterogeneous Anisotropic Plates, *J. Appl. Mech.*, vol. 37, pp. 1031–1036, 1970.
15. E. Carrera, A Class of Two Dimensional Theories for Multilayered Plates Analysis, *Atti Acad. Sci. Torino Mem. Sci. Fis.*, vol. 19–20, pp. 49–87, 1995.
16. E. Carrera, Historical Review of Zig-Zag Theories for Multilayered Plates and Shells, *Appl. Mech. Rev.*, vol. 56, pp. 287–308, 2003.
17. E. Carrera, Theories and Finite Elements for Multilayered Anisotropic, Composite Plates and Shells, *Arch. Computational Meth. Eng.*, vol. 9, pp. 87–140, 2002.
18. J. F. He, Thermoelastic Analysis of Laminated Plates Including Transverse Shear Deformation Effects, *Composite Struct.*, vol. 30, pp. 51–59, 1995.
19. H. Murakami, Assessment of Plate Theories for Treating the Thermomechanical Response of Layered Plates, *Composite Eng.*, vol. 3, no. 2, pp. 137–143, 1993.
20. K. N. Cho, A. G. Striz, and C. W. Bert, Thermal Stress Analysis of Laminate Using Higher-Order Theory in Each Layer, *J. Therm. Stress.*, vol. 12, pp. 321–332, 1989.
21. A. A. Kheider and J. N. Reddy, Thermal Stresses and Deflections of Cross-Ply Laminated Plates using Refined Plate Theories, *J. Therm. Stress.*, vol. 14, pp. 419–438, 1991.
22. S. Srinivas and A. K. Rao, A Note on Flexure of Thick Rectangular Plates and Laminates with Variation of Temperature across the Thickness, *Bull. Acad. Pol. Sci. Ser. Sci. Technol.*, vol. 20, pp. 229–234, 1972.
23. M. N. Bapu Rao, 3D Analysis of Thermally Loaded Thick Plates, *Nucl. Eng. Des.*, vol. 55, pp. 353–361, 1979.
24. K. Bhaskar, T. K. Varadan, and J. S. M. Ali, Thermoelastic Solution for Orthotropic and Anisotropic Composites Laminates, *Composites Part B Eng.*, vol. 27, pp. 415–420, 1986.

25. J. S. M. Ali, K. Bhaskar, and T. K. Varadan, A New Theory for Accurate Thermal/Mechanical Flexural Analysis of Symmetric Laminated Plates, *Composite Struct*., vol. 45, pp. 227–232, 1999.
26. V. B. Tungikar and K. M. Rao, Three Dimensional Exact Solution of Thermal Stresses in Rectangular Composite Laminate, *Composite Struct*., vol. 27, pp. 419–430, 1994.
27. A. K. Noor, Y. H. Kym, and J. M. Peters, Transverse Shear Stresses and Their Sensitivity Coefficients in Multilayered Composite Panels, *AIAA J*., vol. 32, pp. 1259–1269, 1994.
28. M. Savoia and J. N. Reddy, Three Dimensional Thermal Analysis of Laminated Composite Plates, *Int. J. Solids Struct*., vol. 32, pp. 593–608, 1995.
29. S. S. Vel and R. C. Batra, Generalized Plane Strain Thermoelastic Deformation of Laminated Anisotropic Thick Plates, *Int. J. Solids Struct*., vol. 38, pp. 1395–1414, 2001.
30. E. Carrera, An Assessment of Mixed and Classical Theories for Thermal Stress Analysis of Orthotropic Plates, *J. Therm. Stress*., vol. 23, pp. 797–831, 2000.
31. E. Carrera and L. Demasi, Multilayered Finite Plate Element Based on Reissner Mixed Variational Theorem. Part I: Theory; Part II: Numerical Analysis, *Int. J. Numerical Meth. Eng*., vol. 55, pp. 191–231, 253–291, 2002.
32. E. Carrera, Theories and Finite Elements for Multilayered Plates and Shells: A Unified Compact Formulation with Numerical Assessment and Benchmarking, *Arch. Computational Meth. Eng*., vol. 10, pp. 215–296, 2003.
33. J. N. Reddy, *Mechanics of Laminated Composite Plates: Theory and Analysis*, CRC Press, Boca Raton, Fla., 1997.
34. J. N. Reddy, *An Introduction to the Finite Element Method*, 2nd ed., McGraw-Hill, San Francisco, 1993.
35. T. J. R. Hughes, *The Finite Element Method: Linear Static and Dynamic Finite Element Analysis*, Dover, San Francisco, 2000.
36. E. Carrera, Developments, Ideas and Evaluations Based upon the Reissner's Mixed Variational Theorem in the Modeling of Multilayered Plates and Shells, *Appl. Mech. Rev*., vol. 54, pp. 301–329, 2001.
37. E. Carrera, Temperature Profile Influence on Layered Plates Response Considering Classical and Advanced Theories, *AIAA J*., vol. 9, pp. 1885–1896, 2002.

APPENDIX A: EXPLICIT FORM OF THE MATERIAL COEFFICIENTS IN THE LAMINATE REFERENCE SYSTEM

Considering a rectangular unidirectional fiber reinforced lamina as the one in Figure 14, two different reference systems can be defined: the material one (1, 2, 3) and the laminate one (x, y, z). The 3-axis and z-axis are coincident and oriented toward the reader's eye. The material reference systems can be obtained rotating counterclockwise the lamina system by an angle Ψ. As stated above, in order to analyze the full laminate, the constitutive equation has to be written in the laminate reference system. In so doing, new material coefficients (untilded ones) are obtained and they have to be related to the ones given in the material reference system (tilded ones) and the angle of rotation of the fibers. Here, all the coefficients appearing in the rotated constitutive equation (1) are explicitly given for an orthotropic lamina. The following notations are made for all the sections:

$$c = \cos(\Psi) \quad s = \sin(\Psi)$$

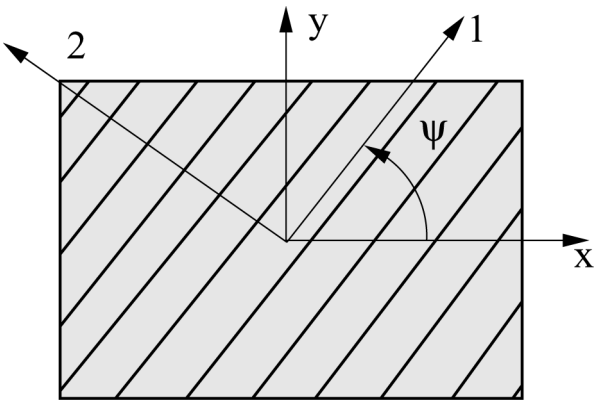

Figure 14 Reference systems for a unidirectional fiber reinforced lamina.

Relation between Elastic Coefficients in the Material and Laminate Reference Systems

$$C_{11} = \widetilde{C}_{11}c^4 + 2\left(\widetilde{C}_{12} + 2\widetilde{C}_{66}\right)c^2s^2 + \widetilde{C}_{22}s^4$$

$$C_{12} = \left(\widetilde{C}_{11} + \widetilde{C}_{22} - 4\widetilde{C}_{66}\right)c^2s^2 + \widetilde{C}_{12}\left(c^4 + s^4\right)$$

$$C_{13} = \widetilde{C}_{13}c^2 + \widetilde{C}_{23}s^2$$

$$C_{16} = -\widetilde{C}_{22}cs^3 + \widetilde{C}_{11}c^3s - \left(\widetilde{C}_{12} + 2\widetilde{C}_{66}\right)cs\left(c^2 - s^2\right)$$

$$C_{22} = \widetilde{C}_{11}s^4 + 2\left(\widetilde{C}_{12} + 2\widetilde{C}_{66}\right)c^2s^2 + \widetilde{C}_{22}c^4$$

$$C_{23} = \widetilde{C}_{13}s^2 + \widetilde{C}_{23}c^2$$

$$C_{33} = \widetilde{C}_{33}$$

$$C_{26} = -\widetilde{C}_{22}c^3s + \widetilde{C}_{11}cs^3 + \left(\widetilde{C}_{12} + 2\widetilde{C}_{66}\right)cs\left(c^2 - s^2\right)$$

$$C_{36} = \left(\widetilde{C}_{13} - \widetilde{C}_{23}\right)cs$$

$$C_{44} = \widetilde{C}_{44}c^2 + \widetilde{C}_{55}s^2$$

$$C_{45} = \left(\widetilde{C}_{55} - \widetilde{C}_{44}\right) cs$$

$$C_{55} = \widetilde{C}_{55} c^2 + \widetilde{C}_{44} s^2$$

$$C_{66} = \left(\widetilde{C}_{11} + \widetilde{C}_{22} - 2\widetilde{C}_{12}\right) c^2 s^2 + \widetilde{C}_{66} \left(c^2 - s^2\right)^2$$

The tilded coefficients are related to the Young's moduli (Y_{ij}), shear moduli (G_{ij}), and Poisson ratios (ν_{ij}) through these relations:

$$\widetilde{C}_{11} = Y_{11} \frac{(1 - \nu_{23}\nu_{32})}{\Delta}$$

$$\widetilde{C}_{22} = Y_{22} \frac{(1 - \nu_{31}\nu_{13})}{\Delta}$$

$$\widetilde{C}_{33} = Y_{33} \frac{(1 - \nu_{12}\nu_{21})}{\Delta}$$

$$\widetilde{C}_{44} = G_{23}$$

$$\widetilde{C}_{55} = G_{13}$$

$$\widetilde{C}_{66} = G_{12}$$

$$\widetilde{C}_{12} = Y_{11} \frac{(\nu_{21} + \nu_{31}\nu_{23})}{\Delta}$$

$$\widetilde{C}_{13} = Y_{22} \frac{(\nu_{13} + \nu_{12}\nu_{23})}{\Delta}$$

$$\widetilde{C}_{23} = Y_{33} \frac{(\nu_{23} + \nu_{21}\nu_{13})}{\Delta}$$

where $\Delta = 1 - \nu_{12}\nu_{21} - \nu_{23}\nu_{32} - \nu_{31}\nu_{13} - 2\nu_{21}\nu_{32}\nu_{13}$ and remembering also:

$$\frac{\nu_{ij}}{Y_{ii}} = \frac{\nu_{ji}}{Y_{jj}} \quad (i,\ j = 1,\ 2,\ 3)$$

That is the relation that garantees the symmetry of $\widetilde{C}$ so that $\widetilde{C}_{kl} = \widetilde{C}_{kl} \quad (k, l = 1, 2, \ldots, 6)$

Relation between Stress-Temperature Coefficients in the Material and Laminate Reference Systems

Stress-temperature coefficients in the material reference system can be found via the coefficients of thermal expansion $\widetilde{\alpha}_j$

$$\widetilde{\lambda}_i = \widetilde{C}_{ij}\widetilde{\alpha}_j$$

with $i,\ j = 1, \ldots, 6$. The previous relation in the case of an orthotropic material for which $\widetilde{\alpha}_4 = \widetilde{\alpha}_5 = \widetilde{\alpha}_6 = 0$ gives the following values:

$$\begin{aligned}
\widetilde{\lambda}_1 &= \widetilde{C}_{11}\widetilde{\alpha}_1 + \widetilde{C}_{12}\widetilde{\alpha}_2 + \widetilde{C}_{13}\widetilde{\alpha}_3 \\
\widetilde{\lambda}_2 &= \widetilde{C}_{12}\widetilde{\alpha}_1 + \widetilde{C}_{22}\widetilde{\alpha}_2 + \widetilde{C}_{23}\widetilde{\alpha}_3 \\
\widetilde{\lambda}_1 &= \widetilde{C}_{13}\widetilde{\alpha}_1 + \widetilde{C}_{23}\widetilde{\alpha}_2 + \widetilde{C}_{33}\widetilde{\alpha}_3
\end{aligned}$$

The coefficients of thermal expansion in the laminate reference system can be easily evaluated via the following relations:

$$\alpha_1 = \widetilde{\alpha}_1 c^2 + \widetilde{\alpha}_2 s^2$$

$$\alpha_2 = \widetilde{\alpha}_1 s^2 + \widetilde{\alpha}_2 c^2$$

$$\alpha_3 = \widetilde{\alpha}_3$$

$$\alpha_4 = 0$$

$$\alpha_5 = 0$$

$$\alpha_6 = 2(\widetilde{\alpha}_1 - \widetilde{\alpha}_2)cs$$

And finally the stress-temperature coefficients in the laminate coordinate system are give by the following equation:

$$\lambda_i = C_{ij}\alpha_j$$

or in explicit as:

$$\lambda_1 = C_{11}\alpha_1 + C_{12}\alpha_2 + C_{13}\alpha_3 + C_{16}\alpha_6$$

$$\lambda_2 = C_{12}\alpha_1 + C_{22}\alpha_2 + C_{23}\alpha_3 + C_{26}\alpha_6$$

$$\lambda_3 = C_{13}\alpha_1 + C_{23}\alpha_2 + C_{33}\alpha_3 + C_{36}\alpha_6$$

$$\lambda_6 = C_{16}\alpha_1 + C_{26}\alpha_2 + C_{36}\alpha_3 + C_{66}\alpha_6$$